New evidence of glacier darkening in the Ortles-Cevedale group from Landsat observations

Davide Fugazza[1], Antonella Senese[1], Roberto Sergio Azzoni[1], Maurizio Maugeri[1], Davide Maragno[1], Guglielmina Adele Diolaiuti[1]

1 Department of Environmental Science and Policy, Università degli studi di Milano, 20133, Milan, Italy

Correspondence to: Davide Fugazza (davide.fugazza@unimi.it)

Abstract

Glacier darkening, or the decrease in glacier albedo over time, has been reported for glaciers in several parts of the world. In this study, we use data from the Landsat archive spanning back to 1984 to investigate the long-term evolution of surface albedo in the ablation area of 15 selected glaciers in the Ortles-Cevedale group, Central Italian Alps, and determine rates and magnitude of darkening. We calculate albedo trends using all available images acquired between 1984 and 2011, by filtering for cloud and snow cover. To confirm that the trends are robust, we perform tests on three pseudo-invariant calibration sites located outside glaciers, ruling out an influence of sensor degradation or varying solar geometry. All 15 investigated glaciers show a decrease in the albedo, which is significant at the 95% (99%) confidence level for 14 (12) glaciers. Albedo trends range between -0.001 y^{-1} and -0.006 y^{-1}, with an average of -0.003 y^{-1}.

We compare our results with previous research in the study area to evaluate the effects of increasing supraglacial debris and climate change on the decrease in albedo; the first appears particularly important for some glaciers and we hypothesize glacier darkening might be caused by a combination of these two factors.

Keywords

Albedo, Alpine glaciers, glacier darkening, remote sensing, Landsat

1 Introduction

Albedo determines the amount of solar radiation absorbed at the glacier surface, and is one of the primary drivers of melt on Alpine glaciers (Oerlemans et al., 2009; Senese et al., 2012a), Himalayan glaciers (Ming et al., 2012) and the Greenland Ice Sheet (Tedesco et al., 2011; 2016). Albedo is highest for fresh snow and decreases through snow metamorphism, the presence of liquid water and

of impurities in ice and snow (Cuffey and Paterson, 2010). A number of studies using point observations (Takeuchi et al., 2003; Oerlemans et al., 2009; Qu et al., 2014; Lutz et al., 2014) or remote sensing (Ming et al., 2012; Mernild et al., 2014; Wang et al., 2014) have shown a recent decrease in ice/snow albedo, or darkening, in several mountain ranges of the world, but the scale and rates of this darkening are still an open issue. Two mechanisms have been primarily held responsible for glacier/ice sheet darkening: higher temperatures and increase in light-absorbing impurities (LAI). The first leads to enhanced melt, the reduction in accumulation areas and exposure of bare ice, promoting a further ice-albedo feedback (Tedesco et al., 2011). Impurities include aerosols such as mineral and organic dust and black carbon (Casey, 2012; Painter et al., 2013; Goelles et al., 2015; Di Mauro et al., 2018), algae (Uetake et al., 2010; Ganey et al., 2017), yeasts (Turchetti et al., 2008) and cryoconite (Hodson et al., 2007; Franzetti et al., 2017a). The increase in the extent of supraglacial rock debris, both fine (Azzoni et al., 2016) and thick (Casey et al., 2012; Reid et al., 2012), also causes widespread darkening, although melt enhancement only occurs below a critical thickness threshold (Bocchiola et al., 2015).

Most long-term albedo studies using remote sensing take advantage from MODIS products at daily or 8-day resolution. These were used to investigate variations e.g. in Hindu Kush Himalayas (Ming et al., 2015), French Alps (Dumont et al., 2014), Svalbard (Moller and Moller, 2017) and Greenland (Mernild et al., 2014; Tedesco et al., 2016). The spatial resolution of MODIS data however is too coarse for most glaciers in the Alps. Landsat data are also available at 30 m resolution since the 1980s. However, few studies of long-term trends in glacier albedo have used this dataset (Naegeli et al., 2019) because of i) Landsat temporal resolution of 16 days, further reduced in practice by clouds/seasonal snow cover and data gaps (Tolnai et al., 2016), ii) the failure of Landsat 7 ETM+ scan line corrector in 2003 causing no-data stripes in ETM+ scenes (Storey et al., 2005), and iii) the lack of standard albedo products unlike those available from MODIS. In spite of these shortcomings, Landsat data represent a unique archive and their potential to investigate long-term albedo trends should be fully exploited. In this study, we used Landsat data between 1984 and 2011 (28 years) to

investigate variations in surface albedo of the ablation area for glaciers in the Lombardy side of Ortles-Cevedale, an important group of the Italian Alps. This mountain group includes Forni Glacier, one of the largest Italian valley glaciers (approximately 11 km^2), and several important glaciers with different sizes, aspects and geometries, thus offering a picture typical of the Italian glaciation. Our aim is to quantify the magnitude and rate of glacier darkening in the ablation area, which has implications for the glacier energy and mass balance. To this end, we analysed the albedo of both bare and buried ice as the increase in supraglacial debris is reported as one of the main causes of glacier darkening (Azzoni et al., 2018).

2 Study Area

The Lombardy side of the Ortles-Cevedale group (46° 27’ N, 10° 37’ E, Central Italian Alps), part of the Adda River basin, hosted 55 glaciers in 2012 (see Fig. 1), covering 25.56 km^2 (Azzoni et al., 2018), with elevations between approximately 2500 m a.s.l. and 3760 m a.s.l. (Fugazza et al., 2018). Nearly half of the total glacier area belongs to Forni Glacier (46° 23’ N, 10° 35’ E), the largest in the region and one of the widest in the Italian Alps (Smiraglia et al., 2015). Glacier meltwater here sustains hydroelectric energy production during the summer months (D’Agata et al., 2018) and glaciers are an important asset of the tourism sector (Garavaglia et al., 2012; Fugazza et al., 2018), owing to their location inside Stelvio National Park (approximately 600 km^2 area within Lombardy), one of the most important protected areas in Italy. The park area includes several sites of community importance, among which Forni Glacier. Owing to its scenic, scientific and naturalistic values, this glacier is also mentioned in the Lombardy Region List of Geosites (Diolaiuti & Smiraglia, 2010).

Glacier shrinkage in the study area has been continuous since the Little Ice Age, with very high retreat rates in the past decades and an increase in the number of glaciers due to fragmentation (from 49 in 2007, D’Agata et al., 2014; D’Agata et al., 2018, to 55 in 2012, Azzoni et al., 2018). Between 2003 and 2012, Azzoni et al. (2018) reported a 14% decrease (4.50 km^2) in glacier area and a 13% increase

in supraglacial debris cover (2.87 km^2). Between 1981 and 2007, D'Agata et al. (2018) estimated a glacier retreat of 42%, a mean surface lowering of -0.70 m y^{-1} and a significant decrease in glacier volume (-766 x 10^6 m^3).

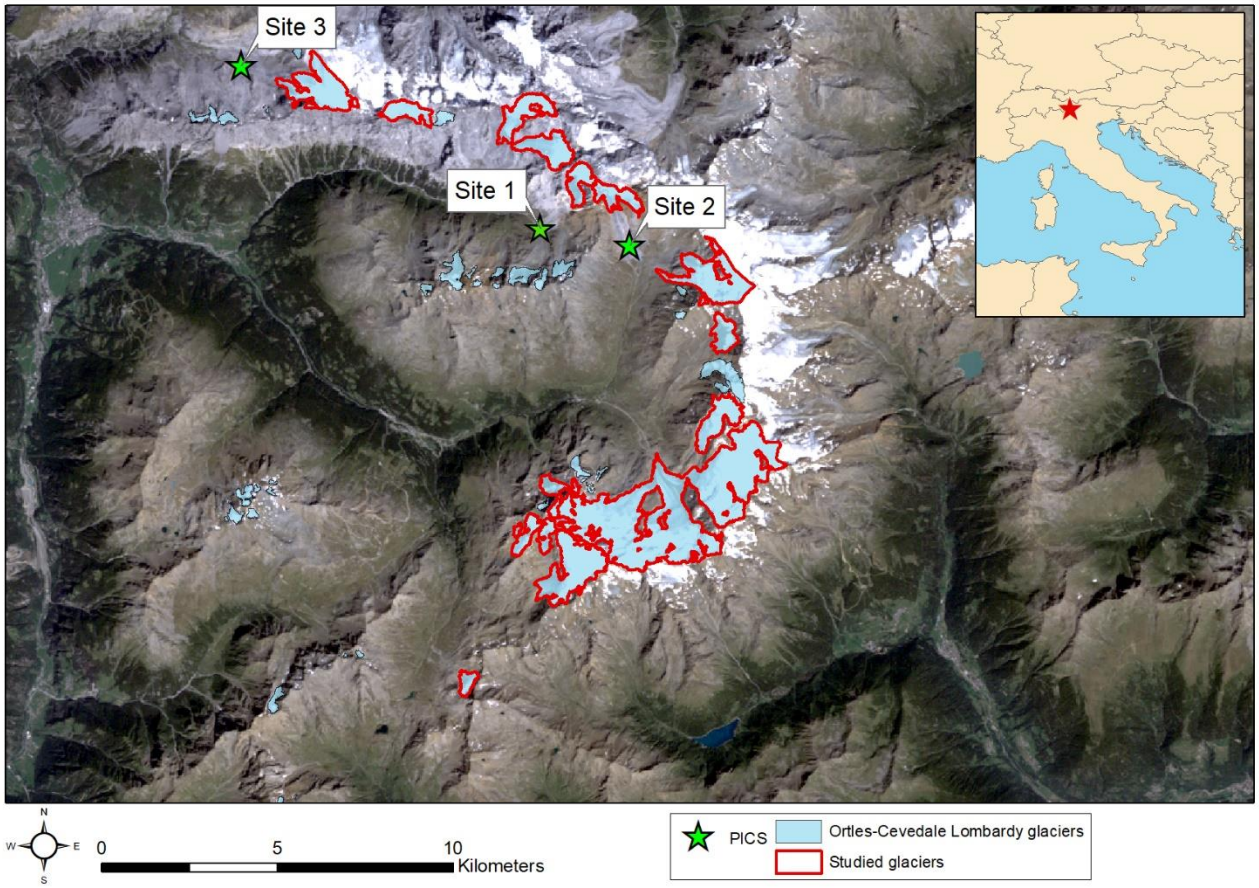

Figure 1: Glaciers of the Lombardy side of Ortles-Cevedale group and their location within Italy. Investigated glaciers are shown in red. Pseudo-invariant calibration sites (PICS) are also shown. Background image is a true-colour composite from a Landsat 5 TM scene of 21/08/2011.

3 Data and Methods

3.1 Albedo Extraction

We downloaded from USGS 48 Landsat Collection 1 L1T images acquired by Landsat 4 TM, Landsat 5 TM and Landsat 7 ETM+ between 1984 and 2011, selecting scenes from 15th July to 30th September, when the glacier ablation area is more likely to be free of snow. Although Landsat 7 ETM+ scenes after 2003 show evidence of striping, the study area lies at the centre of the scene and thus is unaffected. Landsat 7 ETM+ acquired further images after 2011 but no snow- and cloud-free images were available in 2012 and more recent scenes were not processed because of the present unavailability of accurate glacier outlines post this year. All images were processed to estimate the albedo following the methodology developed by Klok et al. (2003) and validated over Forni Glacier, i.e. the largest in the group, by Fugazza et al. (2016). The algorithm is fully described in these studies, so only a summary is given here (see Fig. 2):

- Landsat raw digital numbers from bands 2 and 4 are converted to radiance and Top-of-Atmosphere (TOA) reflectance, using the coefficients found in the scene metadata.
- TOA reflectance is converted to bottom-of-atmosphere (BOA) reflectance using the 6S radiative transfer code (Vermote et al., 1997). The inputs for atmospheric correction are vertical profiles of temperature, water vapour and ozone, and values of aerosol optical thickness. The vertical profiles of temperature and water vapour were obtained from the Milano Linate radiosonde, while ozone data were taken from observations of the SBUV (until 2009) and GOME (after 2009) satellites, using the six points closest to the study area spatially interpolated using inverse distance weighting. Aerosol data were obtained through a climatological dataset from the Jungfraujoch station (see Fugazza et al., 2016). A modified version of Py6S (Wilson et al., 2013) was used to derive all the parameters automatically.
- BOA reflectance is corrected for the effects of topography to yield the reflectance of a tilted surface, by considering the incident angle of direct solar radiation as well as diffuse solar radiation and radiation reflected from neighbouring areas reaching the target. A Digital Elevation Model (DEM) is used as input while the direct and diffuse components of solar radiation are taken from the 6S output. DEMs from 1981 and 2007 were made available by

Regione Lombardia; we adopted the closest DEM to each image, i.e. images between 1987 and 1990 were processed using the 1981 DEM and images between 2000 and 2011 using the 2007 DEM, each resampled to the 30 m resolution of Landsat L1T data.

- Topographically corrected reflectance is converted to albedo taking into account the effects of anisotropic reflection of glacier ice, using parameterizations depending on the satellite view and azimuth angles, as described by Fugazza et al. (2016).
- The final albedo values in bands 2 and 4 are combined using an empirical parameterization to produce a single broadband albedo value for each pixel. The parameterization has a reported accuracy of 0.009 for the albedo of glacier ice (Knap et al., 1999). As saturation can frequently occur in visible bands; if band 2 is saturated only band 4 is used with a separate parameterization (Knap et al., 1999). If both bands are saturated, the pixel is omitted.

All these steps were performed automatically over each scene taking advantage of GRASS GIS libraries and the Python programming language.

3.2 Time series construction

The construction of a time series for each glacier required further steps to identify optimal scenes for comparison, including the removal of cloud- and snow-covered scenes, and to define a reference ablation area (see Fig. 2). Clouds were automatically classified using the automatic cloud cover assessment (ACCA) procedure (Irish, 2000). For each scene, glaciers with above 10% of cloudy pixels were excluded from the analysis. Since ACCA does not accurately recognize cloud shadows (Fugazza et al., 2016), glaciers contaminated by cloud shadows or residual clouds undetected by ACCA were excluded manually. Glaciers with excessive snow cover (above 50% of their area, determined from the number of pixels with albedo > 0.40) were also discarded. This albedo threshold used to discriminate between ice and snow was chosen based on studies on data acquired by a permanent automatic meteorological station on the surface of the Forni Glacier tongue (Senese et al.,

2012b; 2014). While using this threshold might include dirty/old snow, the amount of pixels with albedo between 0.30 and 0.40 is generally low, below 10% of the total (Fugazza et al., 2016).

After selecting the optimal scenes, the reference ablation area was identified based on the snowline. On each scene, the snowline was determined as the transition zone between albedo values lower and greater than 0.40, and the snowline altitude (SLA, based on the 2007 DEM) was recorded. For each glacier, the lowest SLA was then used in combination with glacier outlines to extract the average albedo of the reference ablation area on selected scenes. The glacier outlines were obtained from manual delineation of an orthophoto of Regione Lombardia acquired in 2012 and are the same used in Azzoni et al. (2018). Using the lowest SLA and outlines from 2012 ensures that the same ablation area was analysed on each scene and the effects of snow cover and glacier retreat, which might show fictitious trends in the albedo, are minimized. Finally, we calculated the uncertainty in each average albedo estimation using the standard error of the mean, i.e. $\sigma_x = \frac{\sigma}{\sqrt{n}}$, where σ is the standard deviation of albedo values of the ablation area and n is the number of pixels considered.

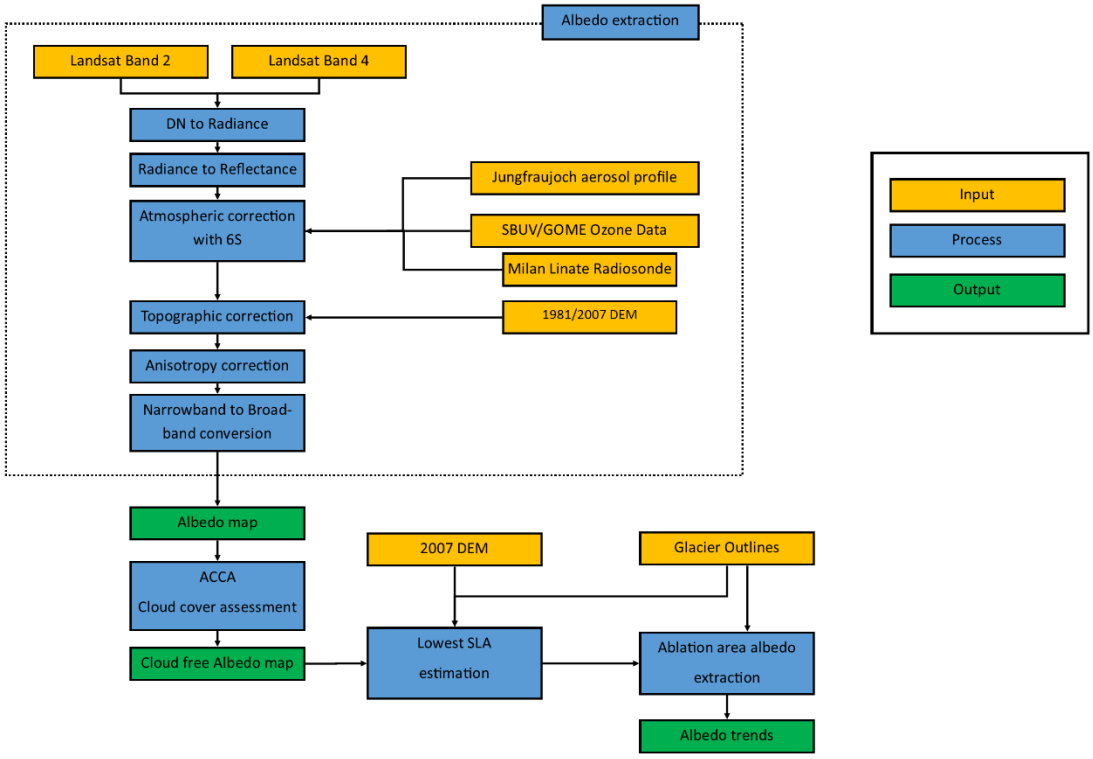

Figure 2: workflow of albedo extraction and trend estimation for individual glaciers.

3.3 Trend determination

To increase the reliability of the results, two criteria were adopted to select Ortles-Cevedale glaciers for estimating their trends: glacier size and availability of scenes. We chose 1) glaciers larger than 0.20 km^2 and 2) glaciers with at least 15 valid scenes. 18 glaciers passed the first criterion, with three glaciers discarded by criterion 2, because of shadowing caused by their unfavourable orientation. This led to a total of 15 investigated glaciers (27% of the total number covering 86% of the total glacier area). On average, 28 scenes were used for trend estimation (see Table 1). For each glacier, we calculated trends using linear regression, using all available dates between 1984 and 2011. We identified albedo change using the slope of linear regression and statistical significance at the 95% and 99% confidence level using a two-tailed student test.

We further analysed Forni Glacier in detail, calculating albedo trends for each individual pixel of the reference ablation area (with elevation lower than 2850 m a.s.l., see Table 1). Beside the size and importance, we selected this glacier because of its long history of research. In recent times, several studies were conducted here aimed at investigating fine and coarse debris cover distribution and evolution (Fugazza et al., 2015; Azzoni et al., 2016; 2018) and evaluating the glacier micrometeorology (e.g. Senese et al., 2018), its energy budget and mass balance (e.g. Senese et al., 2012a). These studies were used as a guide to interpret and understand the albedo trend.

Table 1: Selected glaciers for trend analysis. Area from 2012 glacier outlines. SLA stands for snowline altitude. Numbers I and II indicate fragmentations from a previous glacier.

Glacier	**Area (km^2)**	**Number of scenes**	**Lowest SLA (m a.s.l.)**
Campo I	0.60	27	3050
Cedèc	1.97	35	3100

Cerena I	0.47	28	2800
Dosegù	2.07	31	2950
Forni	10.83	37	2850
Gran Zebrù I	0.64	16	3100
Miniera	0.59	23	3000
Palon de la Mare	1.00	29	3150
Punta Pedranzini I	0.31	23	3200
Rosole	0.56	25	3050
Sforzellina	0.25	20	2850
Tresero	0.47	22	3100
Vitelli	1.70	24	2850
Zebrù I	0.98	37	2950
Zebrù II	0.96	39	2950

182

183

184 **4 Results**

185 **4.1 Mean glacier albedo trends**

186

187 All 15 investigated glaciers show a decrease in the albedo of the reference ablation area between 1984
188 and 2011. The decrease is significant at the 95% (99%) confidence level for 14 (13) glaciers (see Fig.
189 3). The mean albedo trend is -0.003±0.001 y^{-1}, considering both all glaciers and only those with
190 significant trends (95%).

191 Campo I and Zebrù I Glaciers have the largest albedo decrease, with -0.006 y^{-1} (99% confidence).
192 Both glaciers actually show a non-linear behaviour: the albedo of Campo I is stable until about 1996,
193 when it starts decreasing linearly; that of Zebrù I has an abrupt drop in 2004, shifting from an average
194 of 0.23 to 0.11. Other highly negative trends concern Gran Zebrù (-0.005 y^{-1}), Rosole and Sforzellina
195 (both -0.004 y^{-1}), all significant at the 99% confidence level. Rosole Glacier has a large negative
196 change until 2000, while between 2000 and 2011 the albedo is stable around 0.11 and no further
197 change occurs. Other glaciers such as Forni and Zebrù II have smaller negative trends (-0.001 y^{-1} and
198 -0.002 y^{-1}, respectively). Cerena I glacier has a weak negative trend, non-significant at the 95%
199 confidence level.

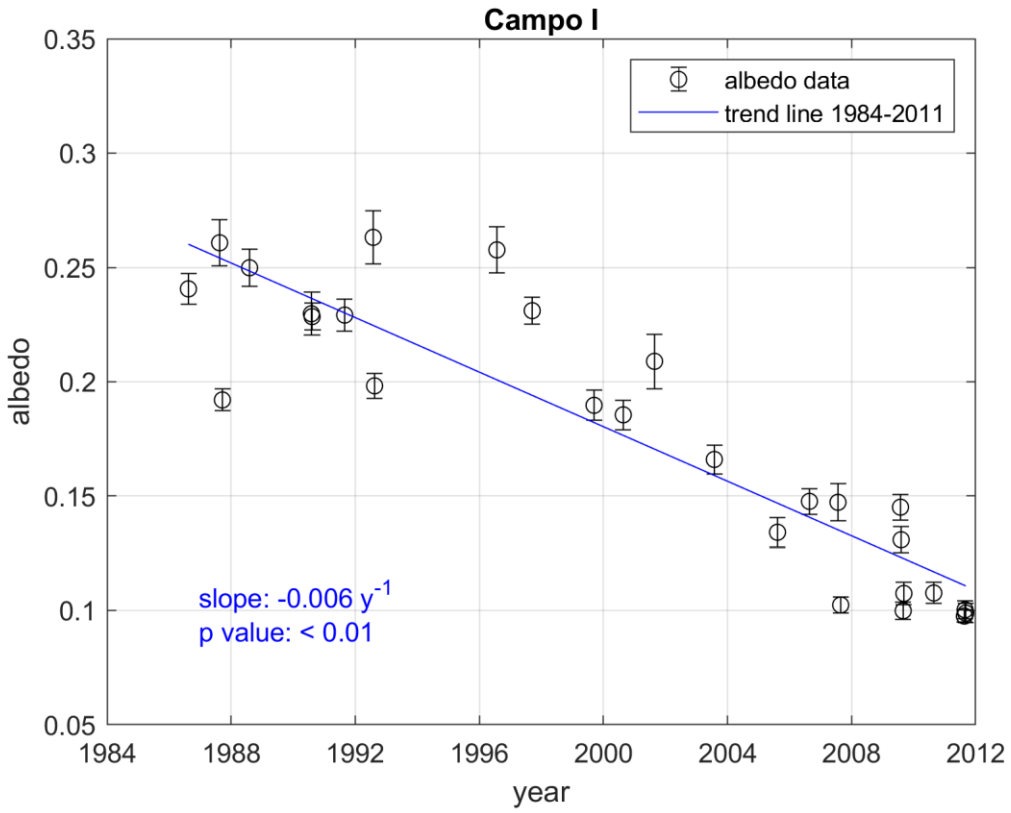
Campo I
albedo data
trend line 1984-2011
slope: -0.006 y-1
p value: < 0.01
albedo
year
0.35
0.3
0.25
0.2
0.15
0.1
0.05
1984
1988
1992
1996
2000
2004
2008
2012

200

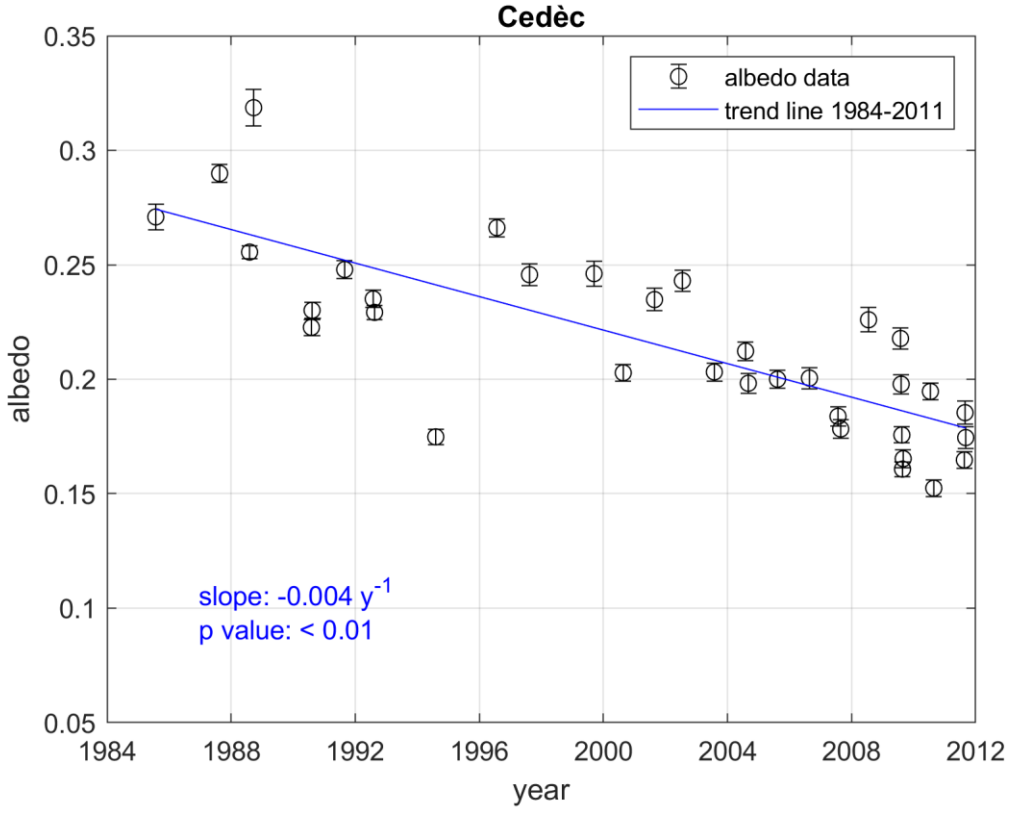
Cedèc
albedo data
trend line 1984-2011
slope: -0.004 y-1
p value: < 0.01
albedo
year
0.35
0.3
0.25
0.2
0.15
0.1
0.05
1984
1988
1992
1996
2000
2004
2008
2012

201

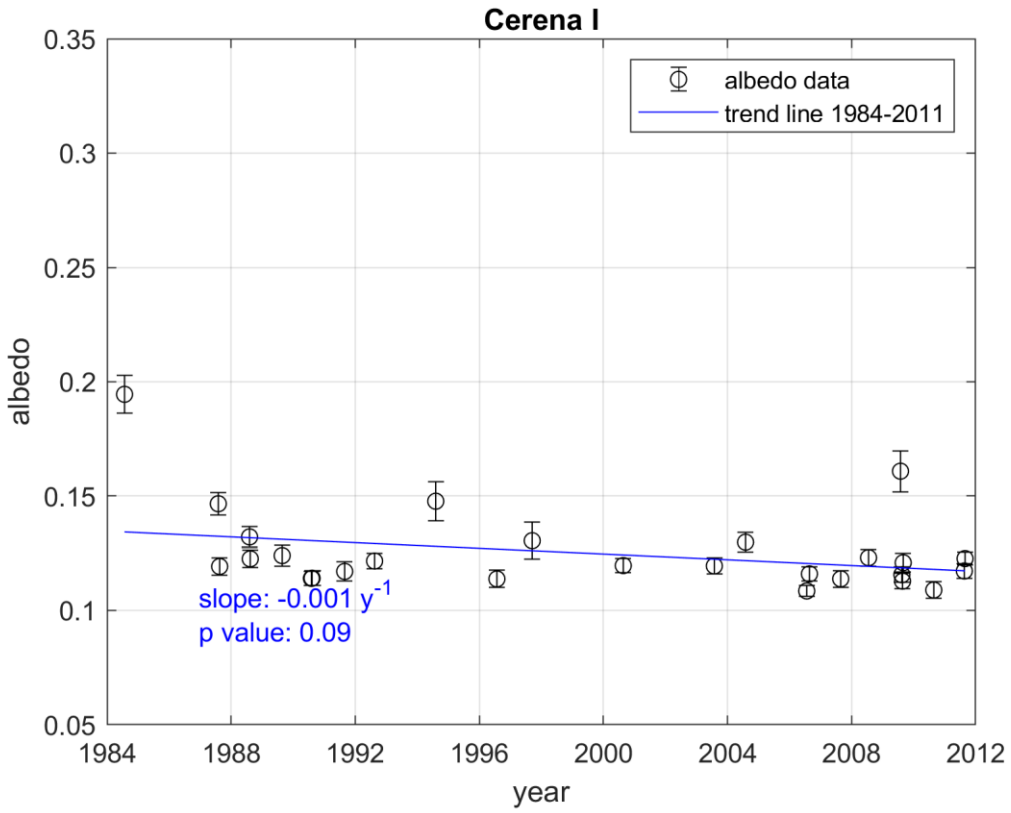
Cerena I
albedo data
trend line 1984-2011
slope: -0.001 y-1
p value: 0.09
albedo
year
0.35
0.3
0.25
0.2
0.15
0.1
0.05
1984
1988
1992
1996
2000
2004
2008
2012

202

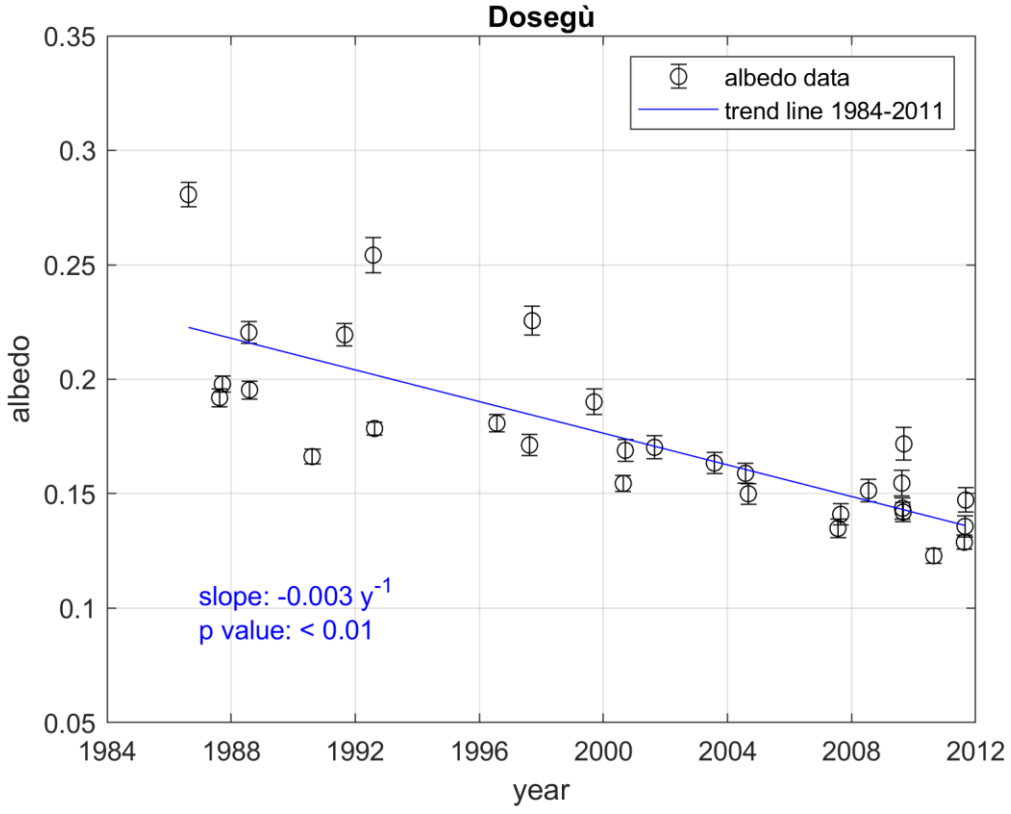
Dosegù
albedo data
trend line 1984-2011
slope: -0.003 y-1
p value: < 0.01
albedo
year
0.35
0.3
0.25
0.2
0.15
0.1
0.05
1984
1988
1992
1996
2000
2004
2008
2012

203

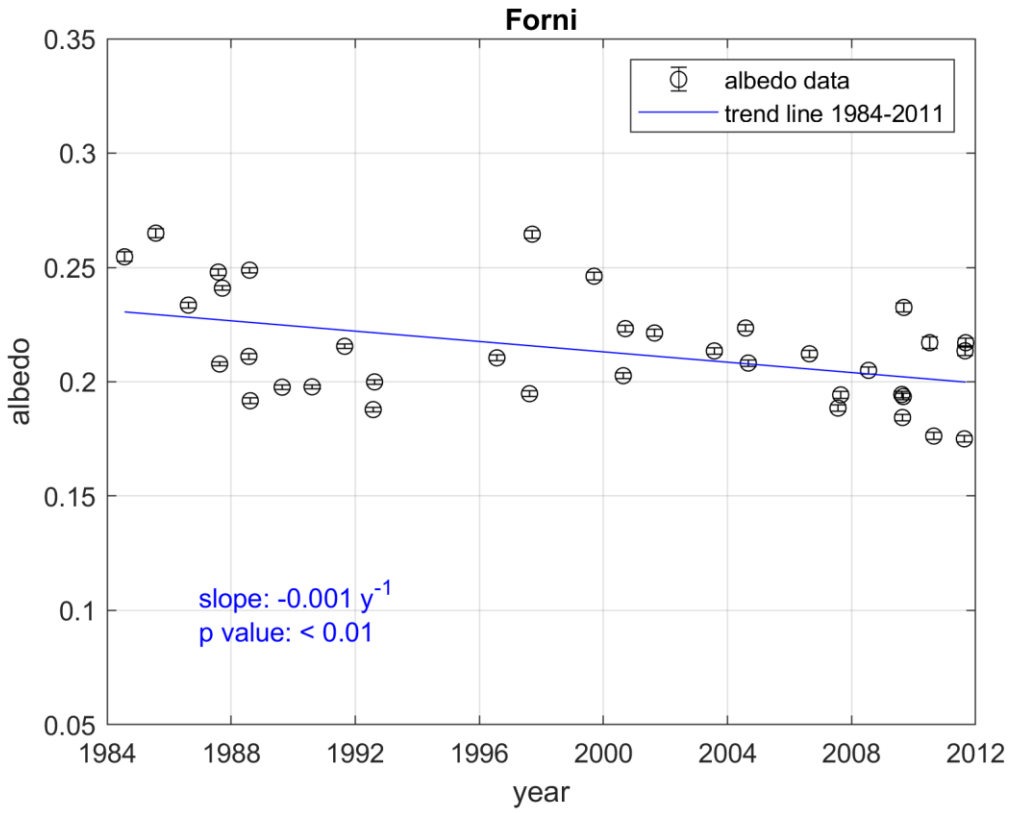
Forni
albedo data
trend line 1984-2011
slope: -0.001 y-1
p value: < 0.01
albedo
year
0.35
0.3
0.25
0.2
0.15
0.1
0.05
1984
1988
1992
1996
2000
2004
2008
2012

204

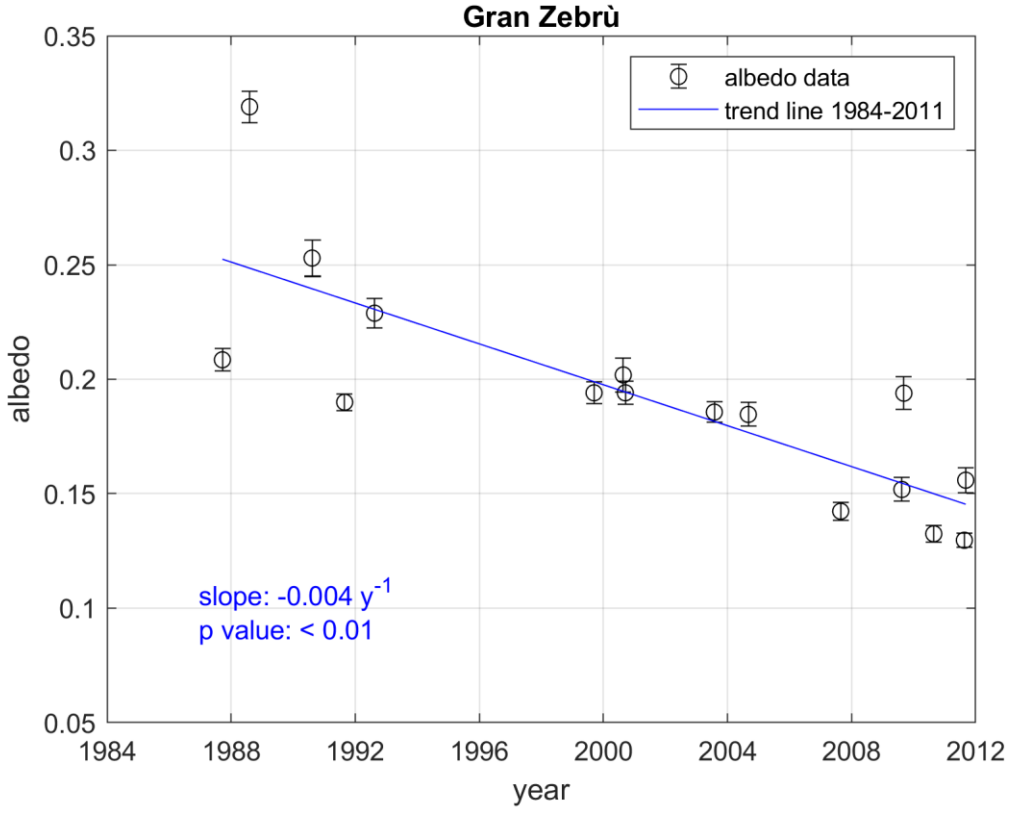
Gran Zebrù
albedo data
trend line 1984-2011
slope: -0.004 y-1
p value: < 0.01
albedo
year
0.35
0.3
0.25
0.2
0.15
0.1
0.05
1984
1988
1992
1996
2000
2004
2008
2012

205

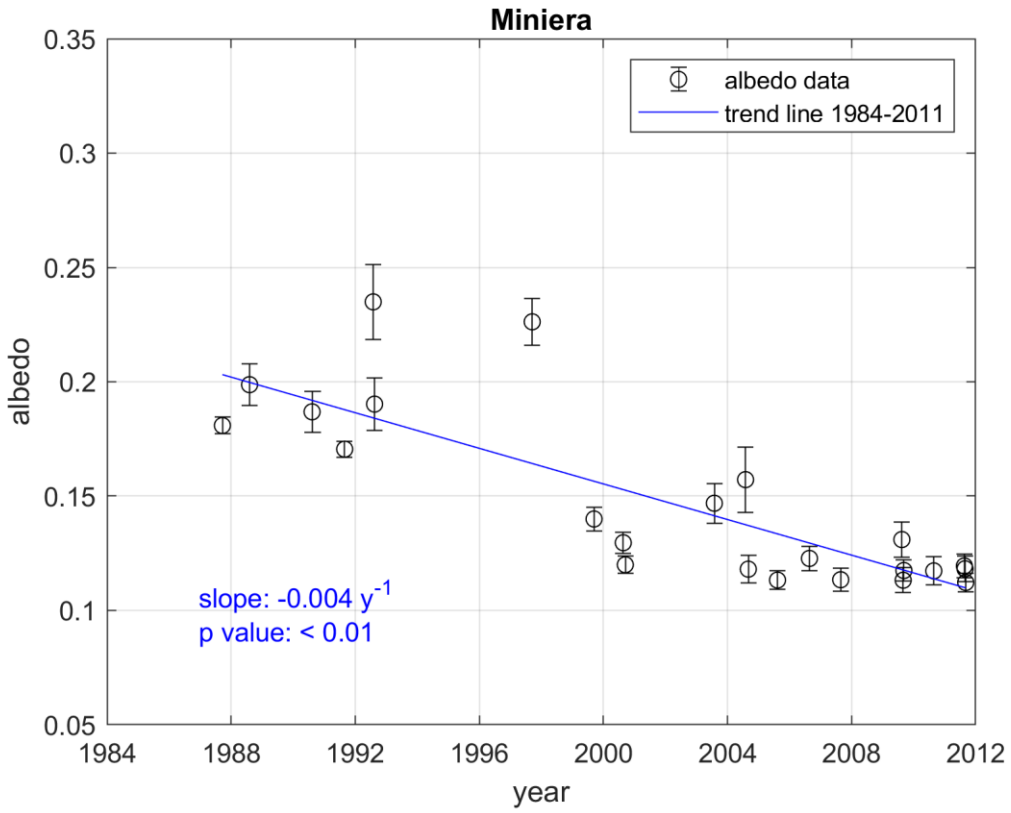
Miniera
albedo data
trend line 1984-2011
slope: -0.004 y-1
p value: < 0.01
albedo
year
0.35
0.3
0.25
0.2
0.15
0.1
0.05
1984
1988
1992
1996
2000
2004
2008
2012

206

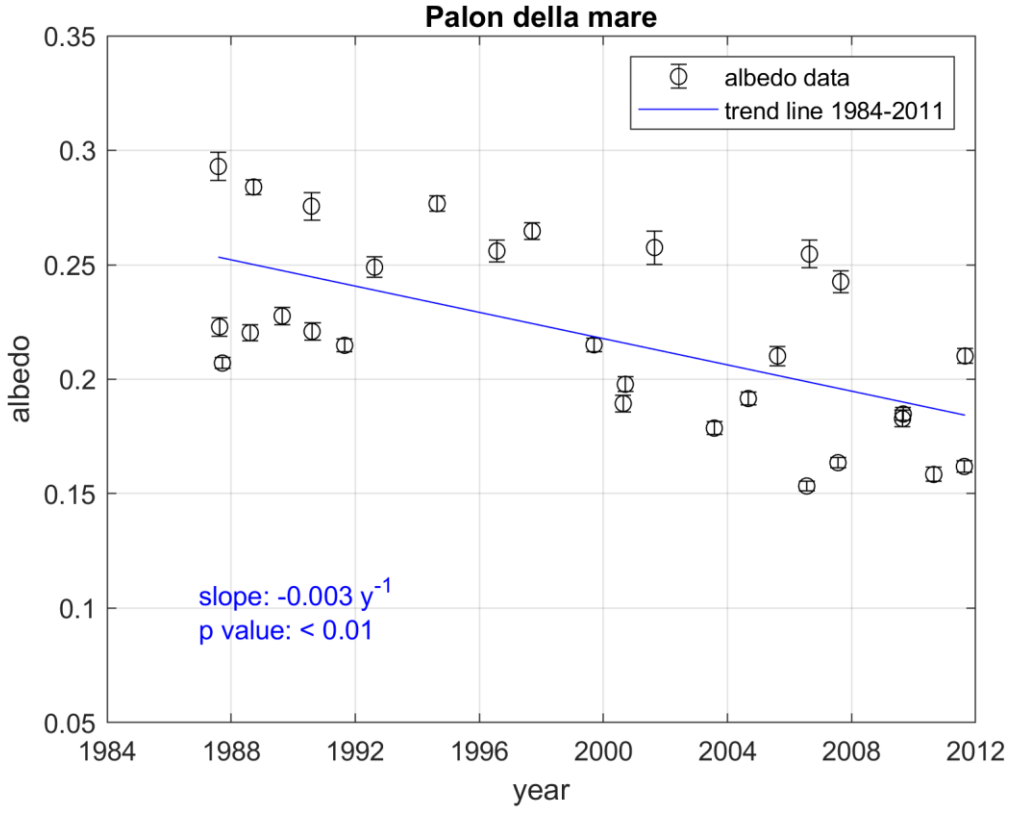
Palon della mare
albedo data
trend line 1984-2011
slope: -0.003 y-1
p value: < 0.01
albedo
year
0.35
0.3
0.25
0.2
0.15
0.1
0.05
1984
1988
1992
1996
2000
2004
2008
2012

207

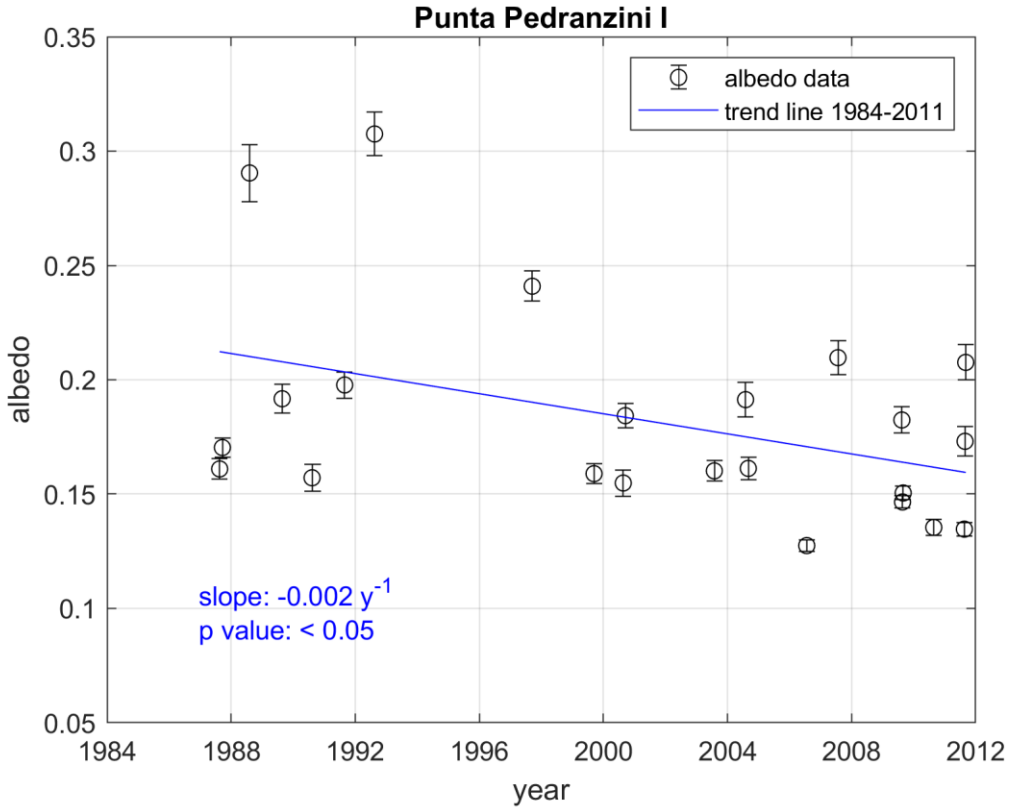
Punta Pedranzini I
albedo data
trend line 1984-2011
slope: -0.002 y-1
p value: < 0.05
albedo
year
0.35
0.3
0.25
0.2
0.15
0.1
0.05
1984
1988
1992
1996
2000
2004
2008
2012

208

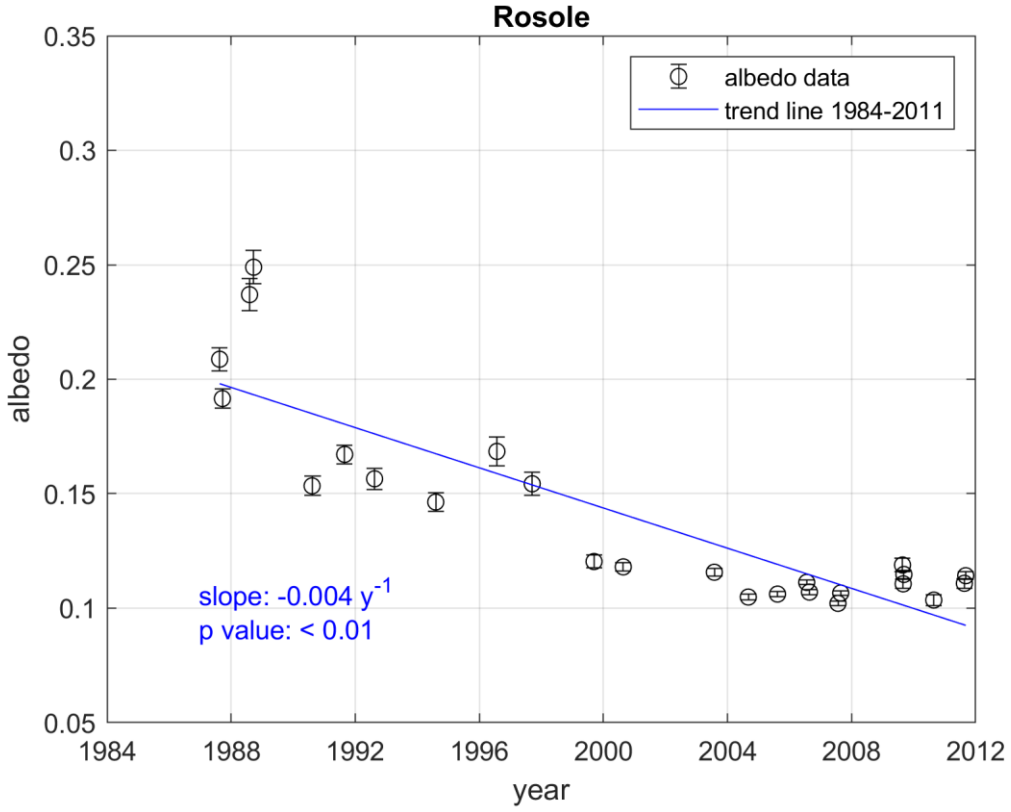
Rosole
albedo data
trend line 1984-2011
slope: -0.004 y-1
p value: < 0.01
albedo
year
0.35
0.3
0.25
0.2
0.15
0.1
0.05
1984
1988
1992
1996
2000
2004
2008
2012

209

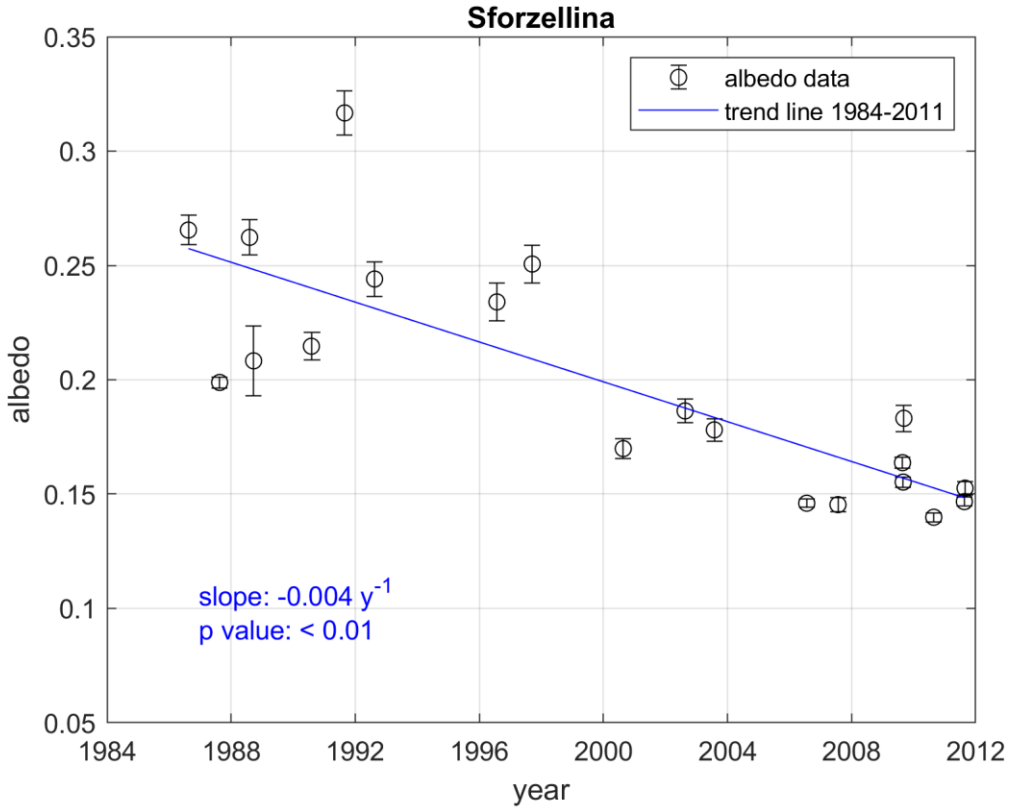
Sforzellina
albedo data
trend line 1984-2011
slope: -0.004 y-1
p value: < 0.01
albedo
year
0.35
0.3
0.25
0.2
0.15
0.1
0.05
1984
1988
1992
1996
2000
2004
2008
2012

210

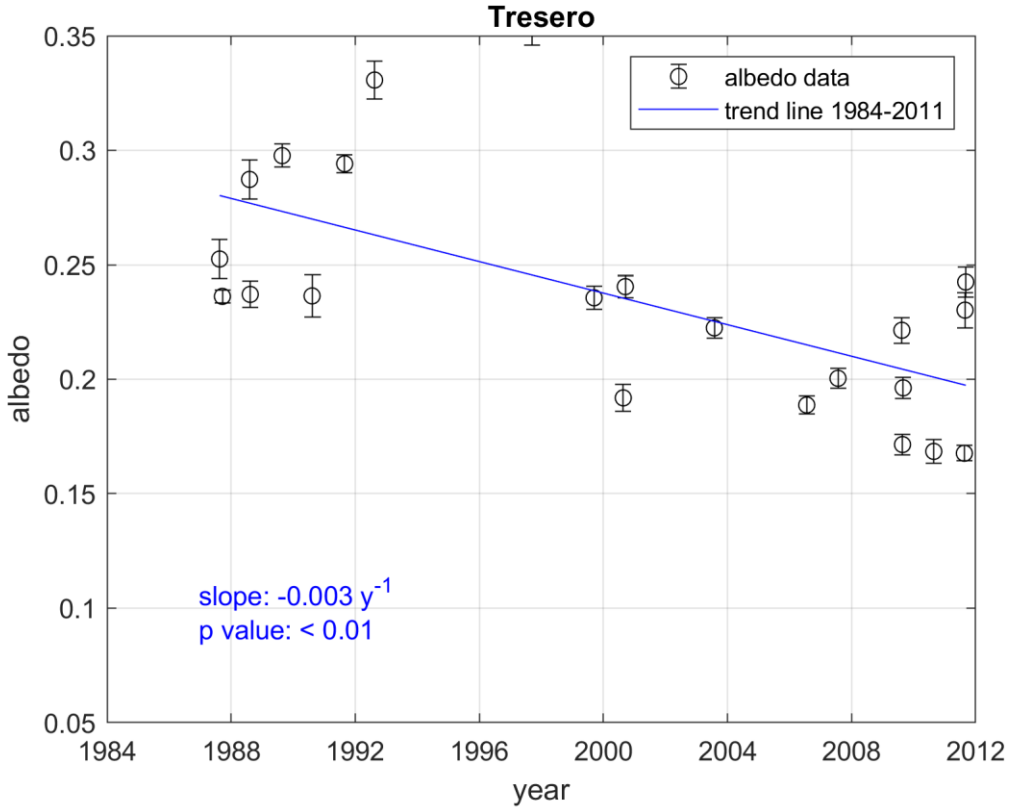
Tresero
albedo data
trend line 1984-2011
slope: -0.003 y-1
p value: < 0.01
albedo
year
0.35
0.3
0.25
0.2
0.15
0.1
0.05
1984
1988
1992
1996
2000
2004
2008
2012

211

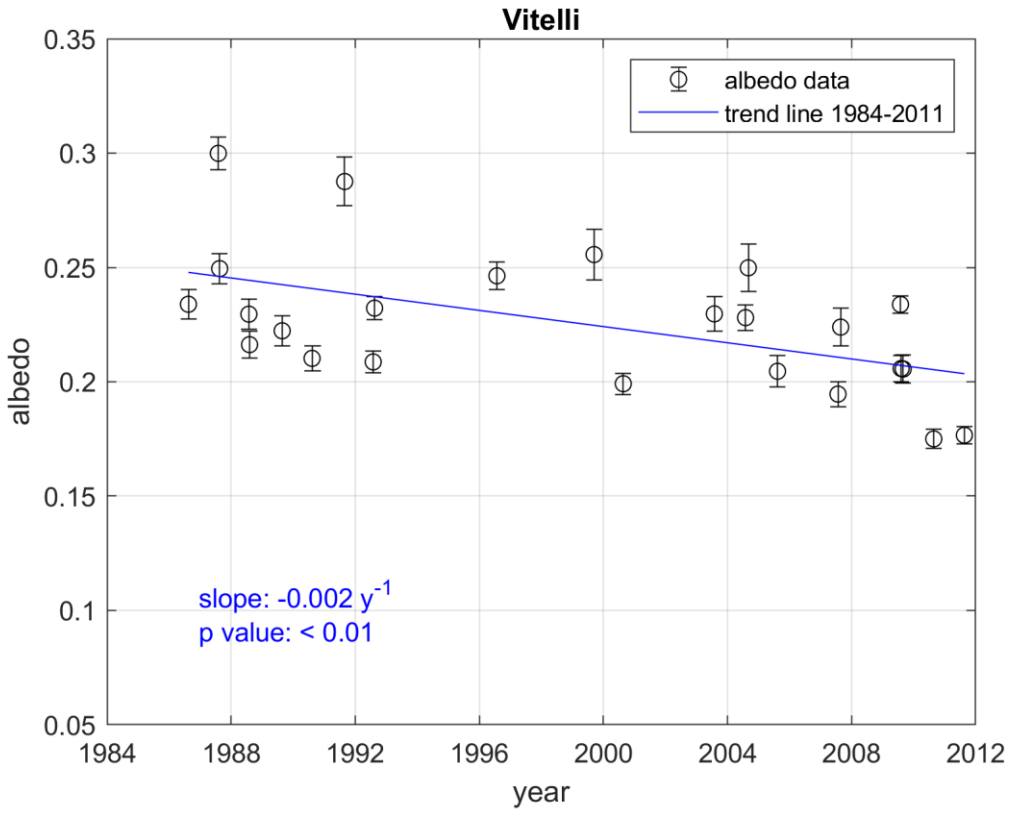
Vitelli
albedo data
trend line 1984-2011
slope: -0.002 y-1
p value: < 0.01
albedo
year
0.35
0.3
0.25
0.2
0.15
0.1
0.05
1984
1988
1992
1996
2000
2004
2008
2012

212

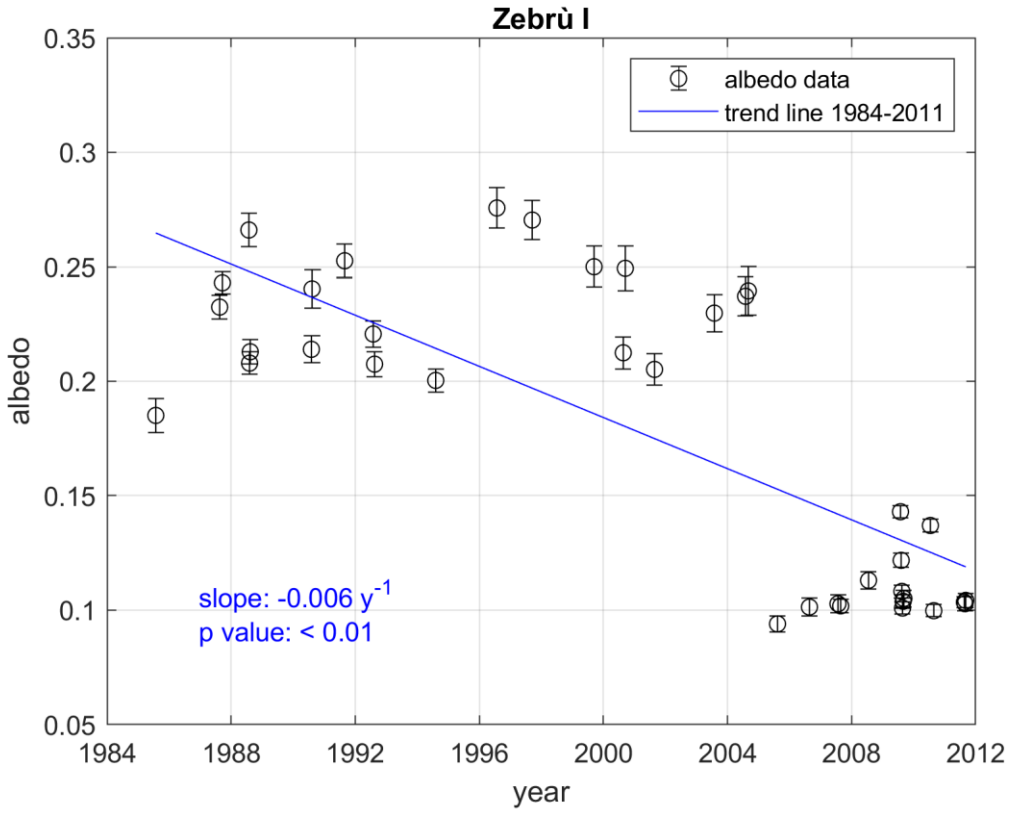
Zebrù I
albedo data
trend line 1984-2011
slope: -0.006 y-1
p value: < 0.01
albedo
year
0.35
0.3
0.25
0.2
0.15
0.1
0.05
1984
1988
1992
1996
2000
2004
2008
2012

213

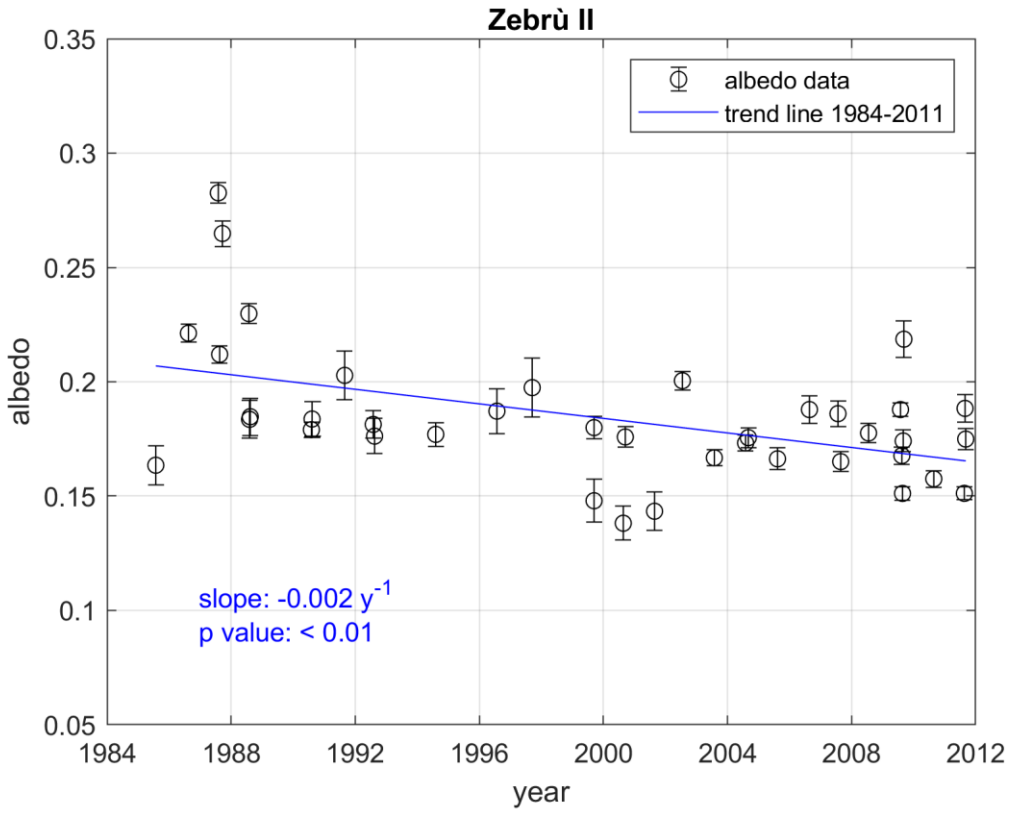

Figure 3: Values of albedo for each scene and yearly albedo trends of the 15 investigated glaciers between 1984 and 2011. The error bars for each value represent the standard error of the average albedo.

4.2. Spatial trends of Forni Glacier

The analysis of Forni Glacier at the pixel scale reveals different patterns (see Fig. 4). Among all pixels, most show a decrease in albedo between 1984 and 2011 (76%, or 77% considering pixels with significant trends). The largest negative trends (< -0.004 y^{-1}, yellow and orange pixels in Fig. 4d) are seen at the terminus (area 1 in Fig. 4d), on the western side of the glacier (area 2) and in two areas at the eastern and western margin at higher elevations (areas 3 and 4), where the albedo decreased by almost -0.010 y^{-1}. Positive trends (up to +0.006 y^{-1}, cyan and blue pixels in Fig. 4d) are instead seen towards the central part of the glacier tongue, relatively close to the western margin (area 5), and on the eastern part of the glacier tongue close to the medial moraine (area 6). The rest of the glacier

shows a rather uniform negative change between -0.001y^{-1} and -0.004 y^{-1}, especially at the terminus, eastern margin at high elevations and upvalley from the medial moraine (compare Fig. 4a and 4d).

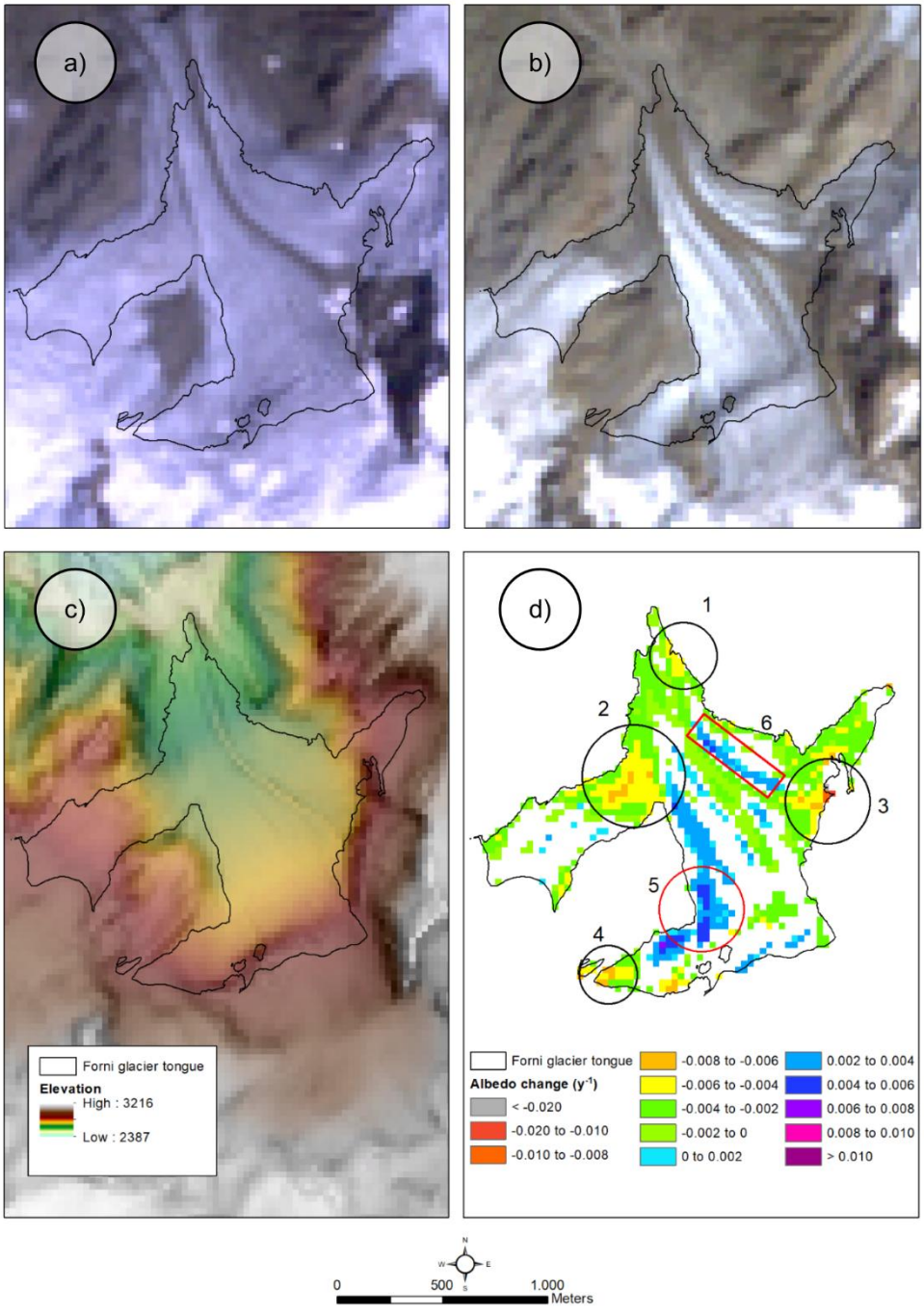

Figure 4: Albedo changes on the tongue of Forni Glacier. a): true color band composite from a Landsat 5 TM scene acquired on 16/08/1986. b): true color band composite from a Landsat 5 TM scene acquired on 21/08/2011. c): elevation representation of the glacier surface based on the 2007 DEM. The sky view factor is shown in transparency to highlight the glacier moraines and topography. d): yearly trends of albedo change for each pixel of the ablation tongue of Forni Glacier between 1984 and 2011. Only trends significant at the 95% level are shown. The outlines of the glacier tongue are from 2012.

5 Discussion

5.1 Uncertainties in the data and trends

To assess the robustness of our trends, we considered three sites, whose albedo is assumed to be stable over time. This allowed us to perform tests to evaluate the influence of sensor degradation, which has an impact on MODIS albedo retrievals (Tedesco et al., 2016), and the varying solar zenith angle (SZA), mentioned by e.g. Schapeman-Strub et al. (2006) for different surfaces. We estimated the albedo using the same methodology employed for glaciers at the three sites (hereafter PICS, pseudo-invariant calibration sites), which are located outside glacier areas on talus slopes (see Fig. 1). The PICS have an average area of 80 pixels, an elevation between 2520 and 2820 m a.s.l. and slope between 13° and 22°. Sites 1 and 3 face northwest while site 2 faces southeast.

Although a slight variability exists in the average albedo values at the PICS, we found no significant trend (at the 95% confidence level) between 1984 and 2011 (see Fig. 5a), in agreement with Li et al. (2018), who reported a high stability of Landsat radiometric data over time, partly thanks to the cross-calibration between Landsat 4/5/7 TM/ETM+. This confirms that using data from these platforms does not introduce uncertainty.

Likewise, no significant trends exist between the albedo and SZA at the three PICS (Fig. 5b); thus, we consider as the maximum uncertainty of the method the value of 0.010 found by Fugazza et al. (2016) for ice surfaces. This value was estimated as the mean absolute error between the albedo calculated with the same approach as this study and the one measured at the automatic weather station (AWS1 Forni) on Forni Glacier.

Considering all glaciers and scenes, the mean standard error in our albedo estimates is 0.005, which gives us further confidence in the overall trends. A small uncertainty might be introduced by mixed pixels, i.e. pixels which are only partly within the glacier boundaries. To minimize the influence of this issue on albedo trends, we chose to use accurate glacier outlines (±0.01%, according to Azzoni et al., 2018) and investigate Landsat images up to the previous year.

A final test was performed to assess the sensitivity of our trends to changes in the ice/snow threshold used to define the reference ablation areas. We recalculated the albedo and trends of each glacier, varying the albedo threshold of 0.40 by ±0.05 (12.5% of the threshold). We found no difference in the significance of trends, while on average the slope of the relationships varies by -0.0002 y^{-1} and +0.0003 y^{-1} for the lower and higher threshold, respectively.

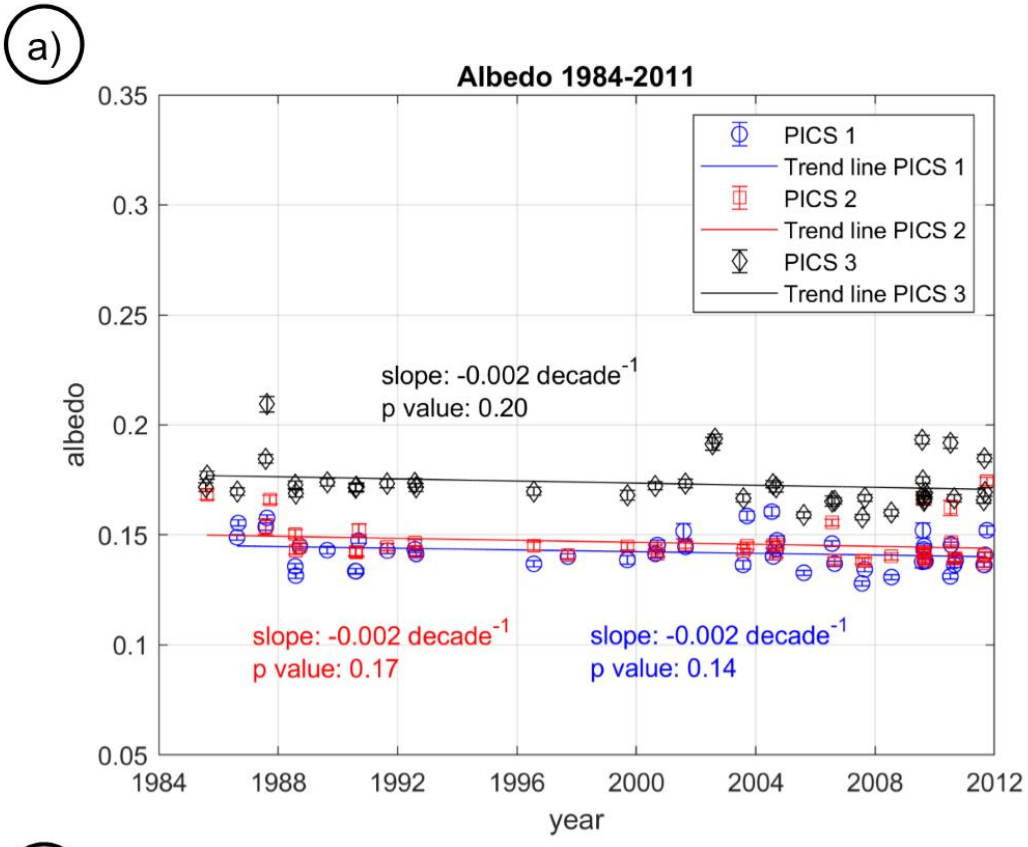
a)
Albedo 1984-2011
PICS 1
Trend line PICS 1
PICS 2
Trend line PICS 2
PICS 3
Trend line PICS 3
slope: -0.002 decade-1
p value: 0.20
slope: -0.002 decade-1
p value: 0.17
slope: -0.002 decade-1
p value: 0.14
albedo
year

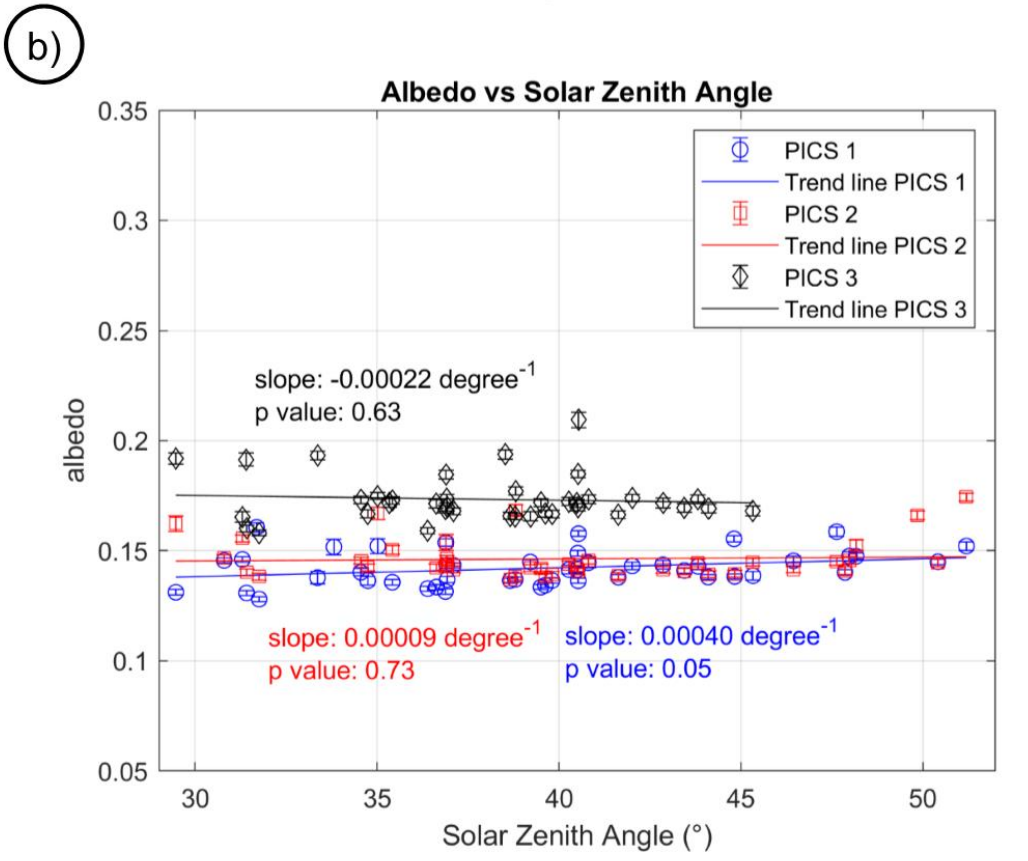
b)
Albedo vs Solar Zenith Angle
PICS 1
Trend line PICS 1
PICS 2
Trend line PICS 2
PICS 3
Trend line PICS 3
slope: -0.00022 degree-1
p value: 0.63
slope: 0.00009 degree-1
p value: 0.73
slope: 0.00040 degree-1
p value: 0.05
albedo
Solar Zenith Angle (°)

Figure 5: tests performed at the three PICS (pseudo-invariant calibration sites). a) Variations in albedo over time between 1984 and 2011. b) Variations in albedo with respect to the solar zenith angle. Error bars represent the standard error.

All these tests suggest that the trends between 1984 and 2011 are consistent and reliable. However, the trends explain between 17% (Punta Pedranzini I Glacier) and 82% (Campo I Glacier) of the variance in albedo, with residuals showing a range up to 0.16 (again at Punta Pedranzini I). This interannual variability might be caused by temporal and meteorological factors. Temporal factors are related to the date of image acquisition, i.e. if the images are acquired later during the ablation season, glacier tongues have a higher chance of being exposed to melting and their albedo might be lower (Senese et al., 2012b). Meteorological factors mainly include rain, fresh snow and clouds. Rain is known to produce a double effect on ice albedo, i.e. a temporary decrease during the event because of the lower albedo of liquid water and a short-lived increase after the event due to washing away of fine sediments (Azzoni et al., 2016). The effects of rainfall are seen up to 4 days later and lead on average to an increase in albedo of +20% with respect to the pre-event values, although increments up to +60% have been reported by Azzoni et al. (2016). In case of summer snowfalls, the albedo of the glacier tongue might be increased by the presence of patches of recent snow ($\alpha > 0.40$) within a pixel. Fugazza et al. (2016) showed that temporal and meteorological factors are tightly linked by analysing data from theAWS1 Forni on the tongue of Forni Glacier to identify rain and snow events before Landsat overpasses. However, their approach cannot be applied here since the AWS1 Forni was installed in 2005. We simply note that as the albedo maps produced from Landsat are snapshots, they might not be entirely representative of inter-annual variability. This can be seen by comparing the albedo of the Forni Glacier retrieved from Landsat with data from the AWS1 Forni (Senese et al., 2012a; 2012b). For example, in 2007 summer snowfall events determined a higher season mean albedo, a pattern not observed in Landsat data (Fig. 3). Beside rain and snow, cloud overpasses during

image acquisition can have an influence on the albedo. Although we excluded clouds and cloud shadows from the analysis through automatic and manual approaches, residual clouds might lead to increased ice albedo since cloud albedo is higher than 0.20 (Hartman, 1994), while cloud shadows may cause unrealistically low values.

5.2 Possible causes of glacier darkening

Glaciers on the Lombardy side of Ortles-Cevedale group saw an increase in supraglacial debris cover between 2003 and 2012 at a rate of +0.32 km^2 y^{-1} (Azzoni et al., 2018), from 16.7% to 30.1% of the total glacier area. In the study by Azzoni et al. (2018) glaciers were investigated in their entirety, while our research is restricted to the glacier ablation areas. To compare the results of the two studies, we used the debris cover maps from Azzoni et al. (2018) and extracted the debris cover of the ablation areas using our definition of SLA for each glacier (see Table 1). We then recalculated albedo trends for each glacier between 2003 and 2011 and compared debris cover changes and albedo trends in the ablation areas (see Fig. 5). We found a significant correlation ($p < 0.05$) of -0.52 between these variables, as more negative albedo trends appear related to a larger increase in debris cover. However, the correlation is strongly leveraged by Zebrù I Glacier, which had a +60% debris cover and a large decrease in albedo, and becomes non-significant if this point is omitted. This glacier saw its ablation area buried in coarse rock debris owing to a rockfall from Thurwieser Spitze in 2004 (Rozman et al., 2004; Armando et al., 2005).

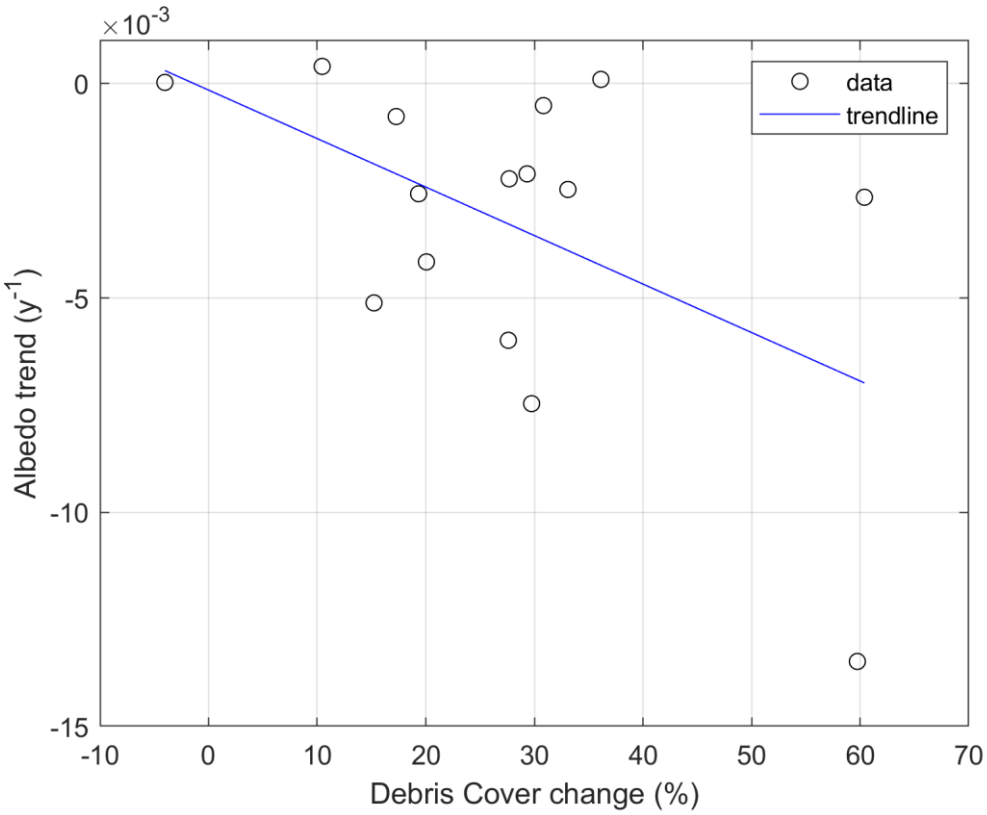

Figure 5: scatter plot of debris cover change 2003-2012 versus annual albedo trends 2003-2011 for each of the 15 selected glaciers.

The glacier with the largest debris cover increase, Miniera, did not undergo an equally large negative trend in the albedo as Zebrù I Glacier. The albedo of this glacier in 2003 was lower than 0.15, a value typical of impurity-rich ice or debris itself, which prevented a further decrease in albedo. The only glacier which underwent a decrease in debris cover between 2003 and 2012, Zebrù II (leftmost point in Figure 5), does not show any significant albedo trend over this period. Note also that the two variables do not share the same period of observation, and that debris classification has an error of 5% (Azzoni et al., 2018), which might introduce some uncertainty.

A more direct evidence of the effect of increasing supraglacial debris cover on albedo trends is seen on Forni Glacier. Comparing the maps of pixelwise albedo trends of the glacier tongue against the findings of Azzoni et al. (2017; 2018) and Fugazza et al. (2015), it appears that the area on the western

328 side of the glacier (where we found a more intense negative albedo variation, see Fig. 4d) underwent
329 a large increase in debris cover, which later favoured the detachment of the western accumulation
330 basin and the glacier tongue (Fugazza et al., 2015). The increase in debris cover shown by Azzoni et
331 al. (2018) at the base of the icefall on the glacier eastern side and at the eastern glacier margin are
332 also seen on our maps (see Fig. 4a,b,d), while the decrease in albedo in longitudinal bands is
333 attributable to the widening of the glacier medial moraines and the formation of new moraine ridges.
334 The causes of increasing debris cover were discussed by Azzoni et al. (2018), who mentioned glacier
335 downwasting and permafrost thawing leading to the debuttressing of rock walls and increased debris
336 input, with further contribution from the emergence of englacial debris. Geomorphological settings
337 (aspect, presence of narrow valleys and steep rock walls) and glacier dynamics also play a role by
338 determining the debris input and the rate of transport. Changes in the Forni Glacier tongue with
339 respect to ice dynamics were also discussed by Azzoni et al. (2017), who reported an increase in the
340 occurrence of crevasses, debris cover and collapsing areas, all possibly contributing to a decrease in
341 albedo, particularly on the eastern and western tongue. Pixels with positive trends might instead
342 represent 1) the shift of glacier moraines, as also found by Naegeli et al. (2019) or 2) the effect of
343 glacier flow transporting cleaner ice downstream.

344 Another factor that might affect the albedo trend is the widespread presence of microbial communities
345 on glaciers. Research conducted on Forni Glacier (Franzetti et al., 2017a;b; Pittino et al., 2018) found
346 an abundance of these organisms in cryoconite that favour intense darkening phoenomena. In
347 particular, the growth and proliferation of these microbes, the entanglement of allochthonous debris,
348 the production of humic substances and photo-protective pigmentation, the enhancement of the
349 longevity of minerals and organic matter on ice surface promote the albedo lowering effect (Cook et
350 al., 2016).

351 The negative trends in glacier albedo can also be linked to the general climatic evolution of the Ortles-
352 Cevedale group. Here, D'Agata et al. (2014) found an increase in the rates of glacier retreat between

1991 and 2007 compared to 1981-1991. They also investigated key climatic variables (i.e. temperature, T, precipitation, P, and snow cover area, SCA), which could have been played an important role in modulating surface albedo through their effects upon glacier evolution. Between 1981 and 2007, significant climate trends include an increase in spring temperatures and a decrease in fall temperatures, a decrease in spring precipitation and winter and spring snow cover. Cannone et al. (2008) also found an increase of +0.5°C in T during 1988–2006 and a decrease in P up to −10% at 2180 m a.s.l. during 1970–2006. The air temperature increase activated a positive feedback, with a consequent increase in both the downward sensible heat flux and the longwave radiation balance (Oerlemans et al., 1998). In addition, this slight increase in T might lead to an earlier snow ablation, as snow melting is sensitive to temperatures above -4.6°C (see Senese et al., 2014). Combined with a lower SCA in winter and spring, this leads to an earlier and longer exposure of glacier ice, especially along the glacier tongues, and therefore a higher probability of LAI deposition causing a larger decrease in albedo during the ablation season.

While our findings reveal a darkening of the ablation tongues of glaciers in the Ortles-Cevedale group, with an average of -0.03 per decade between 1984 and 2011, even higher darkening rates were reported by Oerlemans et al. (2009), who investigated Vedret da Morteratsch, Swiss Alps between 1995 and 2007, using data from the glacier AWS. On this glacier, the decrease in albedo from 0.32 to 0.15 over the observation period was attributed to an increase in the flux of dust, i.e. fine sediments, from the glacier moraines and favoured by the growth of snow algae. However, in other studies of Alpine glaciers, negative albedo trends are less consistent. Naegeli et al. (2019) investigated 39 glaciers from the western and southern Swiss Alps using Landsat data between 1999 and 2016. No significant albedo trends were found at the glacier or regional scale, while 12% of the whole bare ice-area showed negative trends of -0.05 per decade at the 95% confidence level. In the French Alps, Dumont et al. (2012) analysed temporal variations in the albedo of Saint Sorlin Glacier using MODIS data, but no significant decrease in albedo was found between 2000 and 2009.

Outside the Alps, glacier darkening appears more evident. In Svalbard, a high decrease in glacier-wide albedo up to -0.010 per decade was found by Moller and Moller (2017), attributed to a significant rise in temperatures and the consequent increase in the glacier equilibrium line altitudes. Tedesco et al. (2016) reported significant negative trends in Greenland, which were linked to an increase in temperatures, leading to an enhanced melting season, but no evidence of an increase in LAI from the analysis of aerosol optical depth or dust/black carbon sources was found. Conversely, Ming et al. (2012) showed LAIs and dust are partly responsible for the darkening of glaciers in the Himalayas between 2000 and 2009. In a subsequent study (Ming et al., 2015) found a decrease in albedo over the Hindukush, Karakoram, middle and eastern Himalayas, with a negative trend of -0.001 y^{-1} between 1999 and 2011, and more negative trends at elevations between 6000 and 6500 m a.s.l., related to snow melt. In western China, Wang et al. (2014) found a significant albedo trend of -0.005 y^{-1} for glacier n.1 between 2000 and 2011, linked to rising air temperatures and black carbon concentration.

Thus, it appears that air temperature and the associated snow melt are the primary causes of glacier darkening, while LAIs and debris can play a secondary, reinforcing role.

6 Conclusions

In this study, we investigated the temporal evolution of the albedo in the ablation area of glaciers in the Lombardy side of Ortles-Cevedale group, Central Italian Alps. We used Landsat 4, 5 and 7 data acquired since the 1980s to quantify rates and magnitude of change, by calculating albedo trends between 1984 and 2011. We then assessed the robustness of these trends by performing tests on three PICS located outside glaciers and were able to exclude any influence of sensor degradation or varying solar geometry at the time of image acquisition.

We thus found that for 14 glaciers, the albedo decreased significantly during the period of observation. The average yearly change was -0.003 y^{-1} suggesting a consistent darkening effect, with some glaciers such as Zebrù I and Campo reaching -0.006 y^{-1}.

To understand the causes of glacier darkening, we compared our results with those from the studies of Azzoni et al. (2018) and D'Agata et al. (2014). The decrease in albedo appears to be the consequence of the interplay between the changes in the climate of the area, including reduced spring precipitation and an increase in air temperatures, and an increase in supraglacial debris cover which occurred over the past decades. Supraglacial debris cover, either from periglacial or englacial origin, reduces the albedo directly while temperature and precipitation changes lead to a longer exposure of ice during the melt season, reinforcing the effects of debris deposition. The role of supraglacial debris cover is not predominant for all glaciers but appears particularly relevant for Zebrù I Glacier, whose ablation area was buried by a rock avalanche, and Forni Glacier, where the decrease in albedo was prompted by the growth of the glacier moraines and debris deposition on the glacier western side.

Our approach to calculate the albedo is entirely based on the use of open source software and it is mostly automatic except for the removal of cloud shadows and the calculation of the snowline for each glacier, which are based on visual assessment. Provided accurate algorithms to perform these steps are devised, the process could therefore be made entirely automatic and could be replicated to investigate the extent of glacier darkening in other areas. While the creation of a complete dataset including multiple dates per year remains a challenging aspect owing to clouds and snow cover, this is the only approach which potentially allows understanding the evolution of the albedo in detail since the 1980s.

The provision of albedo trends for individual glaciers also opens up possibilities to investigate the impacts of decreased albedo in the glacier ablation area on melt rates and mass balance, both in the Ortles-Cevedale and elsewhere; beside the ablation area, further research could also be conducted on snow and the glacier accumulation basins, to investigate the effects of fine LAIs in these areas. Further

still, the impact of glacier darkening on the tourism sector and the frequentation of high mountain environments could be evaluated. Finally, the seamless integration of Landsat 4-7, Landsat-8 and Sentinel-2 data, not considered in this study, would allow greatly extending the record of observations to the present years and into the future.

Acknowledgments

The authors are thankful to DARA - Department for regional affairs and autonomies – of the Italian presidency of the council of ministers and Levissima Sanpellegrino S.P.A. for funding this research; our gratitude also goes to IIT (Infrastruttura Informatica Territoriale) of Regione Lombardia for providing the 1981 and 2007 DEMs, and Stelvio National Park for permitting data acquisition for research on Forni Glacier.

Competing interests

Declarations of interest: none

Data availability

Landsat TM/ETM+ Collection 1 data are available from USGS repositories at https://earthexplorer.usgs.gov/

The glacier outlines can be requested by writing an email to davide.fugazza@unimi.it

Reference List

Armando, E., Baroni, C., Meneghel, M., 2005. Report of the glaciological survey 2004. Geografia Fisica e Dinamica Quaternaria 28, 233–288.

Azzoni, R.S., Senese, A., Zerboni, A., Maugeri, M., Smiraglia, C., Diolaiuti, G.A., 2016. Estimating ice albedo from fine debris cover quantified by a semi-automatic method: the case study of Forni Glacier, Italian Alps. The Cryosphere 10, 665–679. https://doi.org/10.5194/tc-10-665-2016

448 Azzoni, R.S., Fugazza, D., Zennaro, M., Zucali, M., D'Agata, C., Maragno, D., Cernuschi, M.,
449 Smiraglia, C., Diolaiuti, G.A., 2017. Recent structural evolution of Forni Glacier tongue (Ortles-
450 Cevedale Group, Central Italian Alps). Journal of Maps 13, 870–878.
451 https://doi.org/10.1080/17445647.2017.1394227

452 Azzoni, R.S., Fugazza, D., Zerboni, A., Senese, A., D'Agata, C., Maragno, D., Carzaniga, A.,
453 Cernuschi, M., Diolaiuti, G.A., 2018. Evaluating high-resolution remote sensing data for
454 reconstructing the recent evolution of supra glacial debris: A study in the Central Alps (Stelvio Park,
455 Italy). Progress in Physical Geography: Earth and Environment 42, 3–23.
456 https://doi.org/10.1177/0309133317749434

457 Bocchiola, D., Senese, A., Mihalcea, C., Mosconi, B., D'Agata, C., Smiraglia, C., Diolaiuti, G.A.,
458 2015. An Ablation Model for Debris-Covered Ice: The Case Study of Venerocolo Glacier (italian
459 Alps). Geografia Fisica e Dinamica Quaternaria 38, 113–128.
460 https://doi.org/10.4461/GFDQ.2015.38.11

461 Cannone, N., Diolaiuti, G., Guglielmin, M., Smiraglia, C., 2008. Accelerating Climate Change
462 Impacts on Alpine Glacier Forefield Ecosystems in the European Alps. Ecological Applications 18,
463 637–648. https://doi.org/10.1890/07-1188.1

464 Casey, K.A., Kääb, A., Benn, D.I., 2012. Geochemical characterization of supraglacial debris via in
465 situ and optical remote sensing methods: a case study in Khumbu Himalaya, Nepal. The Cryosphere
466 6, 85–100. https://doi.org/10.5194/tc-6-85-2012

467 Cook, J., Edwards, A., Takeuchi, N., Irvine-Fynn, T., 2016. Cryoconite: The dark biological secret
468 of the cryosphere. Progress in Physical Geography 40, 66–111.
469 https://doi.org/10.1177/0309133315616574

470 Cuffey, K.M., Paterson, W.S.B., 2010. The Physics of Glaciers, 4 edition. ed. Academic Press,
471 Burlington, MA.

D'Agata, C., Bocchiola, D., Maragno, D., Smiraglia, C., Diolaiuti, G.A., 2014. Glacier shrinkage driven by climate change during half a century (1954–2007) in the Ortles-Cevedale group (Stelvio National Park, Lombardy, Italian Alps). Theor Appl Climatol 116, 169–190. https://doi.org/10.1007/s00704-013-0938-5

D'Agata, C., Bocchiola, D., Soncini, A., Maragno, D., Smiraglia, C., Diolaiuti, G.A., 2018. Recent area and volume loss of Alpine glaciers in the Adda River of Italy and their contribution to hydropower production. Cold Regions Science and Technology 148, 172–184. https://doi.org/10.1016/j.coldregions.2017.12.010

Di Mauro, B., Garzonio, R., Rossini, M., Filippa, G., Pogliotti, P., Galvagno, M., Morra di Cella, U., Migliavacca, M., Baccolo, G., Clemenza, M., Delmonte, B., Maggi, V., Dumont, M., Tuzet, F., Lafaysse, M., Morin, S., Cremonese, E., Colombo, R., 2019. Saharan dust events in the European Alps: role in snowmelt and geochemical characterization. The Cryosphere 13, 1147–1165. https://doi.org/10.5194/tc-13-1147-2019

Diolaiuti, G., Smiraglia, C., 2010. Changing glaciers in a changing climate: how vanishing geomorphosites have been driving deep changes in mountain landscapes and environments. Géomorphologie : relief, processus, environnement 16, 131–152. https://doi.org/10.4000/geomorphologie.7882

Dumont, M., Gardelle, J., Sirguey, P., Guillot, A., Six, D., Rabatel, A., Arnaud, Y., 2012. Linking glacier annual mass balance and glacier albedo retrieved from MODIS data. The Cryosphere 6, 1527–1539. https://doi.org/10.5194/tc-6-1527-2012

Franzetti, A., Navarra, F., Tagliaferri, I., Gandolfi, I., Bestetti, G., Minora, U., Azzoni, R.S., Diolaiuti, G., Smiraglia, C., Ambrosini, R., 2017a. Temporal variability of bacterial communities in cryoconite on an alpine glacier. Environ Microbiol Rep 9, 71–78. https://doi.org/10.1111/1758-2229.12499

Franzetti, A., Navarra, F., Tagliaferri, I., Gandolfi, I., Bestetti, G., Minora, U., Azzoni, R.S., Diolaiuti, G., Smiraglia, C., Ambrosini, R., 2017b. Potential sources of bacteria colonizing the cryoconite of an Alpine glacier. PlosOne 12. e0174786. https://doi.org/10.1371/journal.pone.0174786

Fugazza, D., Senese, A., Azzoni, R.S., Smiraglia, C., Cernuschi, M., Severi, D., Diolaiuti, G.A., 2015. High-Resolution Mapping of Glacier Surface Features. the Uav Survey of the Forni Glacier (stelvio National Park, Italy). Geografia Fisica e Dinamica Quaternaria 25–33. https://doi.org/10.4461/GFDQ.2015.38.03

Fugazza, D., Senese, A., Azzoni, R.S., Maugeri, M., Diolaiuti, G.A., 2016. Spatial distribution of surface albedo at the Forni Glacier (Stelvio National Park, Central Italian Alps). Cold Regions Science and Technology 125, 128–137. https://doi.org/10.1016/j.coldregions.2016.02.006

Fugazza, D., Scaioni, M., Corti, M., D'Agata, C., Azzoni, R.S., Cernuschi, M., Smiraglia, C., Diolaiuti, G.A., 2018. Combination of UAV and terrestrial photogrammetry to assess rapid glacier evolution and map glacier hazards. Nat. Hazards Earth Syst. Sci. 18, 1055–1071. https://doi.org/10.5194/nhess-18-1055-2018

Ganey, G.Q., Loso, M.G., Burgess, A.B., Dial, R.J., 2017. The role of microbes in snowmelt and radiative forcing on an Alaskan icefield. Nature Geoscience 10, 754–759. https://doi.org/10.1038/ngeo3027

Garavaglia, V., Diolaiuti, G., Smiraglia, C., Pasquale, V., Pelfini, M., 2012. Evaluating Tourist Perception of Environmental Changes as a Contribution to Managing Natural Resources in Glacierized Areas: A Case Study of the Forni Glacier (Stelvio National Park, Italian Alps). Environmental Management 50, 1125–1138. https://doi.org/10.1007/s00267-012-9948-9

Goelles, T., Bøggild, C.E., Greve, R., 2015. Ice sheet mass loss caused by dust and black carbon accumulation. The Cryosphere 9, 1845–1856. https://doi.org/10.5194/tc-9-1845-2015

Hartmann, D.L., 1994. Global Physical Climatology. Academic Press, San Diego. 411pp.

519 Hodson, A., Anesio, A.M., Ng, F., Watson, R., Quirk, J., Irvine-Fynn, T., Dye, A., Clark, C.D.,
520 McCloy, P., Kohler, J., Sattler, B., 2007. A glacier respires: Quantifying the distribution and
521 respiration CO2 flux of cryoconite across an entire Arctic supraglacial ecosystem. Journal of
522 Geophysical Research: Biosciences 112.

523 Irish, R.R., 2000. Landsat 7 automatic cloud cover assessment, in: Algorithms for Multispectral,
524 Hyperspectral, and Ultraspectral Imagery VI. Presented at the Algorithms for Multispectral,
525 Hyperspectral, and Ultraspectral Imagery VI, International Society for Optics and Photonics, pp. 348–
526 356. https://doi.org/10.1117/12.410358

527 Klok, E.J., Greuell, W., Oerlemans, J., 2003. Temporal and spatial variation of the surface albedo of
528 Morteratschgletscher, Switzerland, as derived from 12 Landsat images. Journal of Glaciology 49,
529 491–502. https://doi.org/10.3189/172756503781830395

530 Knap, W.H., Reijmer, C.H., Oerlemans, J., 1999. Narrowband to broadband conversion of Landsat
531 TM glacier albedos. International Journal of Remote Sensing 20, 2091–2110.
532 https://doi.org/10.1080/014311699212362

533 Li, S., Wang, W., Ganguly, S., Nemani, R.R., 2018. Radiometric Characteristics of the Landsat
534 Collection 1 Dataset. Advances in Remote Sensing 07, 203–217.
535 https://doi.org/10.4236/ars.2018.73014

536 Lutz, S., Anesio, A.M., Jorge Villar, S.E., Benning, L.G., 2014. Variations of algal communities
537 cause darkening of a Greenland glacier. FEMS Microbiol. Ecol. 89, 402–414.
538 https://doi.org/10.1111/1574-6941.12351

539 Mernild, S.H., Malmros, J.K., Yde, J.C., Wilson, R., Knudsen, N.T., Hanna, E., Fausto, R.S., As, D.
540 van, 2014. Albedo decline on Greenland's Mittivakkat Gletscher in a warming climate. International
541 Journal of Climatology 35, 2294–2307. https://doi.org/10.1002/joc.4128

Ming, J., Du, Z., Xiao, C., Xu, X., Zhang, D., 2012. Darkening of the mid-Himalaya glaciers since 2000 and the potential causes. Environ. Res. Lett. 7, 014021. https://doi.org/10.1088/1748-9326/7/1/014021

Ming, J., Wang, Y., Du, Z., Zhang, T., Guo, W., Xiao, C., Xu, X., Ding, M., Zhang, D., Yang, W., 2015. Widespread Albedo Decreasing and Induced Melting of Himalayan Snow and Ice in the Early 21st Century. PLOS ONE 10. https://doi.org/10.1371/journal.pone.0126235

Möller, M., Möller, R., 2017. Modeling glacier-surface albedo across Svalbard for the 1979–2015 period: The HiRSvaC500-α data set. Journal of Advances in Modeling Earth Systems 9, 404–422. https://doi.org/10.1002/2016MS000752

Naegeli, K., Huss, M., Hoelzle, M., 2019. Change detection of bare-ice albedo in the Swiss Alps. The Cryosphere 13, 397–412. https://doi.org/10.5194/tc-13-397-2019

Oerlemans, J., Anderson, B., Hubbard, A., Huybrechts, P., Jóhannesson, T., Knap, W.H., Schmeits, M., Stroeven, A.P., Wal, R.S.W. van de, Wallinga, J., Zuo, Z., 1998. Modelling the response of glaciers to climate warming. Climate Dynamics 14, 267–274. https://doi.org/10.1007/s003820050222

Oerlemans, J., Giesen, R.H., Van Den Broeke, M.R., 2009. Retreating alpine glaciers: increased melt rates due to accumulation of dust (Vadret da Morteratsch, Switzerland). Journal of Glaciology 55, 729–736. https://doi.org/10.3189/002214309789470969

Painter, T.H., Flanner, M.G., Kaser, G., Marzeion, B., VanCuren, R.A., Abdalati, W., 2013. End of the Little Ice Age in the Alps forced by industrial black carbon. Proceedings of the National Academy of Sciences 110, 15216–15221. https://doi.org/10.1073/pnas.1302570110

Pittino, F., Maglio, M., Gandolfi, I., Azzoni, R.S., Diolaiuti, G., Ambrosini, R., Franzetti, A., 2018. Bacterial communities of cryoconite holes of a temperate alpine glacier show both seasonal trends and year-to-year variability. Annals of Glaciology 1–9. https://doi.org/10.1017/aog.2018.16

Qu, B., Ming, J., Kang, S.-C., Zhang, G.-S., Li, Y.-W., Li, C.-D., Zhao, S.-Y., Ji, Z.-M., Cao, J.-J., 2014. The decreasing albedo of the Zhadang glacier on western Nyainqentanglha and the role of light-absorbing impurities. Atmospheric Chemistry and Physics 14, 11117–11128. https://doi.org/10.5194/acp-14-11117-2014

Reid, T.D., Carenzo, M., Pellicciotti, F., Brock, B.W., 2012. Including debris cover effects in a distributed model of glacier ablation. Journal of Geophysical Research: Atmospheres 117, 1–15. https://doi.org/10.1029/2012JD017795

Rozman, J., Rožič, A., Budkovič, A., Budkovič, T., 2004. Rockfall in the southern wall of Punta Thurwieser (Italy) on September 18th, 2004. Geologija 47, 221–232. https://doi.org/10.5474/geologija.2004.017

Schaepman-Strub, G., Schaepman, M.E., Painter, T.H., Dangel, S., Martonchik, J.V., 2006. Reflectance quantities in optical remote sensing—definitions and case studies. Remote Sensing of Environment 103, 27–42. https://doi.org/10.1016/j.rse.2006.03.002

Senese, A., Diolaiuti, G., Verza, G.P., Smiraglia, C., 2012a. Surface energy budget and melt amount for the years 2009 and 2010 at the Forni Glacier (Italian Alps, Lombardy). Geografia Fisica e Dinamica Quaternaria 35, 69–78.

Senese, A., Diolaiuti, G., Mihalcea, C., Smiraglia, C., 2012b. Energy and Mass Balance of Forni Glacier (Stelvio National Park, Italian Alps) from a Four-Year Meteorological Data Record. Arctic, Antarctic, and Alpine Research 44, 122–134. https://doi.org/10.1657/1938-4246-44.1.122

Senese, A., Maugeri, M., Vuillermoz, E., Smiraglia, C., Diolaiuti, G., 2014. Using daily air temperature thresholds to evaluate snow melting occurrence and amount on Alpine glaciers by T-index models: the case study of the Forni Glacier (Italy). The Cryosphere 8, 1921–1933. https://doi.org/10.5194/tc-8-1921-2014

589 Senese, A., Maugeri, M., Meraldi, E., Verza, G.P., Azzoni, R.S., Compostella, C., Diolaiuti, G., 2018.
590 Estimating the snow water equivalent on a glacierized high elevation site (Forni Glacier, Italy). The
591 Cryosphere 12, 1293–1306. https://doi.org/10.5194/tc-12-1293-2018

592 Smiraglia, P., Azzoni, R.S., D'Agata, C., Maragno, D., Fugazza, D., Diolaiuti, G.A., 2015. The
593 Evolution of the Italian Glaciers from the Previous Data Base to the New Italian Inventory.
594 Preliminary Considerations and Results. Geografia Fisica e Dinamica Quaternaria 38, 79–87.
595 https://doi.org/10.4461/GFDQ.2015.38.08

596 Storey, J., Scaramuzza, P., Schmidt, G., Barsi, J., 2005. Landsat 7 scan line corrector-off gap-filled
597 product development. Presented at the PECORA 16 Conference Proceedings, Sioux Falls, South
598 Dakota, US, pp. 23–27.

599 Takeuchi, N., Kohshima, S., Segawa, T., 2003. Effects of cryoconite and snow algal communities on
600 surface albedo on maritime glaciers in south Alaska. Bulletin of Glaciological Research 20, 21–27.

601 Tedesco, M., Fettweis, X., van den Broeke, M.R., Wal, R.S.W. van de, Smeets, C.J.P.P., Berg, W.J.
602 van de, Serreze, M.C., Box, J.E., 2011. The role of albedo and accumulation in the 2010 melting
603 record in Greenland. Environ. Res. Lett. 6, 014005. https://doi.org/10.1088/1748-9326/6/1/014005

604 Tedesco, M., Doherty, S., Fettweis, X., Alexander, P., Jeyaratnam, J., Stroeve, J., 2016. The
605 darkening of the Greenland ice sheet: trends, drivers, and projections (1981–2100). The Cryosphere
606 10, 477–496. https://doi.org/10.5194/tc-10-477-2016

607 Tolnai, M., Nagy, J.G., Bakó, G., 2016. Spatiotemporal distribution of Landsat imagery of Europe
608 using cloud cover-weighted metadata. Journal of Maps 12, 1084–1088.
609 https://doi.org/10.1080/17445647.2015.1125308

610 Turchetti, B., Buzzini, P., Goretti, M., Branda, E., Diolaiuti, G., D'Agata, C., Smiraglia, C., Vaughan-
611 Martini, A., 2008. Psychrophilic yeasts in glacial environments of Alpine glaciers. FEMS Microbiol.
612 Ecol. 63, 73–83. https://doi.org/10.1111/j.1574-6941.2007.00409.x

Uetake, J., Naganuma, T., Hebsgaard, M.B., Kanda, H., Kohshima, S., 2010. Communities of algae and cyanobacteria on glaciers in west Greenland. Polar Science 4, 71–80. https://doi.org/10.1016/j.polar.2010.03.002

Vermote, E.F., Tanre, D., Deuze, J.L., Herman, M., Morcette, J., 1997. Second Simulation of the Satellite Signal in the Solar Spectrum, 6S: an overview. IEEE Transactions on Geoscience and Remote Sensing 35, 675–686. https://doi.org/10.1109/36.581987

Wang, J., Ye, B., Cui, Y., He, X., Yang, G., 2014. Spatial and temporal variations of albedo on nine glaciers in western China from 2000 to 2011. Hydrological Processes 28, 3454–3465. https://doi.org/10.1002/hyp.9883

Wilson, R.T., 2013. Py6S: A Python interface to the 6S radiative transfer model. Computers & Geosciences 51, 166–171. https://doi.org/10.1016/j.cageo.2012.08.002

Wulder, M.A., White, J.C., Loveland, T.R., Woodcock, C.E., Belward, A.S., Cohen, W.B., Fosnight, E.A., Shaw, J., Masek, J.G., Roy, D.P., 2016. The global Landsat archive: Status, consolidation, and direction. Remote Sensing of Environment 185, 271–283. https://doi.org/10.1016/j.rse.2015.11.032